Continuous atmospheric CO_2, CH_4 and CO measurements at the Observatoire Pérenne de l'Environnement (OPE) station in France from 2011 to 2018

Sébastien Conil[1], Julie Helle[2], Laurent Langrene[1], Olivier Laurent[2], Marc Delmotte[2], Michel Ramonet[2]

[1]DRD/OPE ,Andra, Bure,55290, FRANCE
[2] Laboratoire des Sciences du Climat et de l'Environnement (LSCE/IPSL), UMR CEA-CNRS-UVSQ, Gif-sur-Yvette, France

Correspondence to: Sébastien Conil (sebastien.conil@andra.fr)

Abstract.

Located in North-East France, the Observatoire Pérenne de l'Environnement (OPE) station was built during the Integrated Carbon Observation System (ICOS) Demonstration Experiment to monitor the atmospheric concentration of greenhouse gases. Its continental rural background setting fills the gaps between oceanic or mountain stations and urban stations within the ICOS network. Continuous measurements of several greenhouse gases using high precision spectrometers started in 2011 on a tall tower with three sampling inlets at 10m, 50m and 120m above the ground. The measurements quality is regularly assessed using several complementary approaches based on reference high pressure cylinders, travelling instruments audit and sets of travelling cylinders (so-called cucumber intercomparison). Thanks to the quality assurance strategy recommended by ICOS, the precision of the measurements is within the World Meteorological Organisation compatibility goals for carbon dioxide (CO_2), methane (CH_4) and carbon monoxide (CO). The mixing ratios time series from 2011 to 2018 are used to analyse trends and diurnal and seasonal cycles. The CO_2 and CH_4 annual growth rates are respectively 2.4 ppm/year and 8.8 ppb/year for the measurements at 120m over the investigated period. However, no significant trends have been recorded for the CO mixing ratios. The afternoon mean residuals (defined as the differences between midday observations and a smooth fitted curve) of these three compounds are significantly stronger during the cold period when inter-species correlations are high, compared to the warm period. The variabilities of residuals show a close link with the air mass back-trajectories.

1 Introduction

Since the beginning of the industrial era, the atmospheric concentrations of long lived greenhouse gases (GHG) have been rising. Increases of surface emissions, mostly from human activities, are responsible for this atmospheric GHG's build up. For carbon dioxide (CO_2), the largest climate change contributor, only around half of the additional anthropogenic emissions are retained in the atmosphere, with the remaining 50% being pumped out by the ocean and the land ecosystems (Le Quéré et al., 2018). As for methane (CH_4) the last ten years are characterized by high growth rates at many observation sites, following a period of stable concentrations from 2000 to 2007 (Nisbet et al., 2019; Turner et al., 2019). Monitoring the atmospheric

concentrations of these GHG is of primary importance for the long-term climate monitoring but also for the assessment of surface fluxes. Because they are performed far from anthropogenic sources and/or are located in the free troposphere, remote and mountain atmospheric measurements are needed to assess background concentrations. Such « global scale » data are of great value for monitoring the global atmospheric GHG build-up but also to estimate global scale fluxes. However, they are not designed to capture the regional-scale signals necessary to assess local to regional scale fluxes. The specific purpose of European Integrated Carbon Observation System (ICOS) is to establish and maintain a dense European GHG observations network to monitor long-term changes, assess the carbon cycle and track carbon and GHG fluxes. Inverse atmospheric methods combining tall tower network measurements and transport models are great tools for assessing surface GHG fluxes exchanged with the biosphere and oceans, and to estimate the anthropogenic emissions (Broquet et al., 2013; Kountouris et al., 2018). They also offer independent ways to improve the bottom-up emissions inventories required by the international agreement under the United Nations Framework Convention on Climate Change (Bergamaschi et al., 2018; Leip et al., 2018; Peters et al., 2017).

ICOS was established as a European strategic research infrastructure which will provide the high precision observations needed to quantify the greenhouse gas balance of Europe and adjacent regions. It is now a widespred infrastructure composed of three integrated networks measuring GHG in the atmosphere, over the ocean and at the ecosystem level. Each network is coordinated by a thematic center that performs centralized data processing. One of the key focuses of ICOS is to provide standardized and automated high-precision measurements, which is achieved by using common measurement protocols and standardized instrumentations. In the atmospheric monitoring network, ICOS targets the World Meteorological Organization (WMO) / Global Atmosphere Watch (GAW) compatibility goal (WMO, 2011) within its own network as well as with other international networks. During the preparatory phase from 2008-2013, a demonstration network and new stations were set up with harmonized specifications (Laurent et al., 2017). The Atmospheric Thematic Center (ATC) performs several metrological tests on the analysers and provides technical support and training regarding all aspects of the in situ GHG measurements (Yver Kwok et al., 2015). The ATC is also responsible for the near real time post processing of the measurements (Hazan et al., 2016).

The OPE station was established under a close collaboration between Andra and LSCE as part of the demonstration experiment during 2010 and 2011 following the ICOS atmospheric station specifications. It is a continental regional background station contributing to the actual network by bridging the gap between remote global/mountain station like Mace Head (MHD) or Jungfraujoch (JFJ), and urban stations like Saclay or Heidelberg. The potential of ICOS continuous measurements of CO_2 dry air mole fraction to improve Net Ecosystem Exchange estimates at the mesoscale across Europe was evaluated in Kadygrov et al. (2015). Pison et al. (2018) addressed the potential of the current ICOS European network for estimating methane emissions at the French national scale France.

The main objectives of this paper are to describe the OPE monitoring station, the continuous GHG measurements system, to present its performance characteristic and to draw results from the first eight years of continuous operations.

2 Site description and GHG measurements system

2.1 Site location

The OPE atmospheric station (48.5625°N, 5.50575°E WGS84, 395 m asl) is located on the eastern edge of the Paris Basin in the North-East part of France, western Europe, as shown on Figure 1. The landscape consists of undulated eroded limestone plateaus dissected by a few SE-NW valleys (60 to 80m). The station is on top of the surrounding hills in a rural area with large crop fields, some pastures and forest patches. According to Corine Land Cover 2012, the dominating land cover types in the 25 / 100 km surroundings are Arable land/crops: 39% /44%, Pastures : 14% /18%, Forest : 44% /34%. Based on GEOFLA database from Institut national de l'information géographique et forestière (IGN), the mean population density within a 25 / 100km radius from the station is 26 / 64 (inhab.km^{-2}). The closest small towns are Delouze with 130 people located 1 km to the South-East and Houdelaincourt with 300 people located 2km to the South-West. The closest cities are Saint Dizier (45,000 inhabitants) located 40km away to the West, Bar Le Duc (35, 000 inhab.) 30km at the North-West, Toul (25,000 inhab.) 30km to the East and Nancy (450,000 inhab.) 50km to the East. With 20 000 cars/day, the major road is located 15km to the North (RN4). The station includes a 120m tall tower and two portable and fully equipped modular buildings on a 2ha fenced area. The station infrastructure was built in 2009 and 2010 and the measurements systems started in 2011.

The OPE station is designed to host a complete set of in situ measurements of meteorological parameters, trace gases (CO_2, CH_4, N_2O, CO, O_3, NO_x, SO_2) and particles parameters(size distribution, absorption and diffusion coefficients, number and mass, chemical composition, radioactivity). The station is part of the French aerosol in situ network contributing to ACTRIS and AERONET program. It is part of the IRSN (Institut de Radioprotection et de Sûreté Nucléaire) network for the ambient air radioactivity monitoring. The station also contributes to the french air quality monitoring network and to the European Monitoring and Evaluation Program.

Figure 1: Geographical location of the OPE atmospheric station (left) and aerial photograph illustrating the landscape surrounding the station (right).

2.2 Local meteorology and air masses trajectories

The local meteorology is monitored using three sets of meteorological sensors located at the three measurement levels on the tower (10m, 50m and 120m agl). Standard meteorological parameters, Temperature, Relative Humidity, Pressure and Wind Speed and Direction, are monitored in compliance with ICOS AS specifications. Minute averaged data are logged and used to produce hourly mean fields. In addition there is a ground based weather station operated by Meteo France, the French national weather service providing hourly mean data in compliance with World Meteorological Organization specifications.

The mean annual temperature between 2011 and 2018 was 10.5°C. The minimum temperature was -15,2°C and the maximum temperature was 36.4°C. The cumulated annual precipitations were 829mm on average. Two local wind regimes are predominant, a south/westerly regime and an east/north easterly regime.

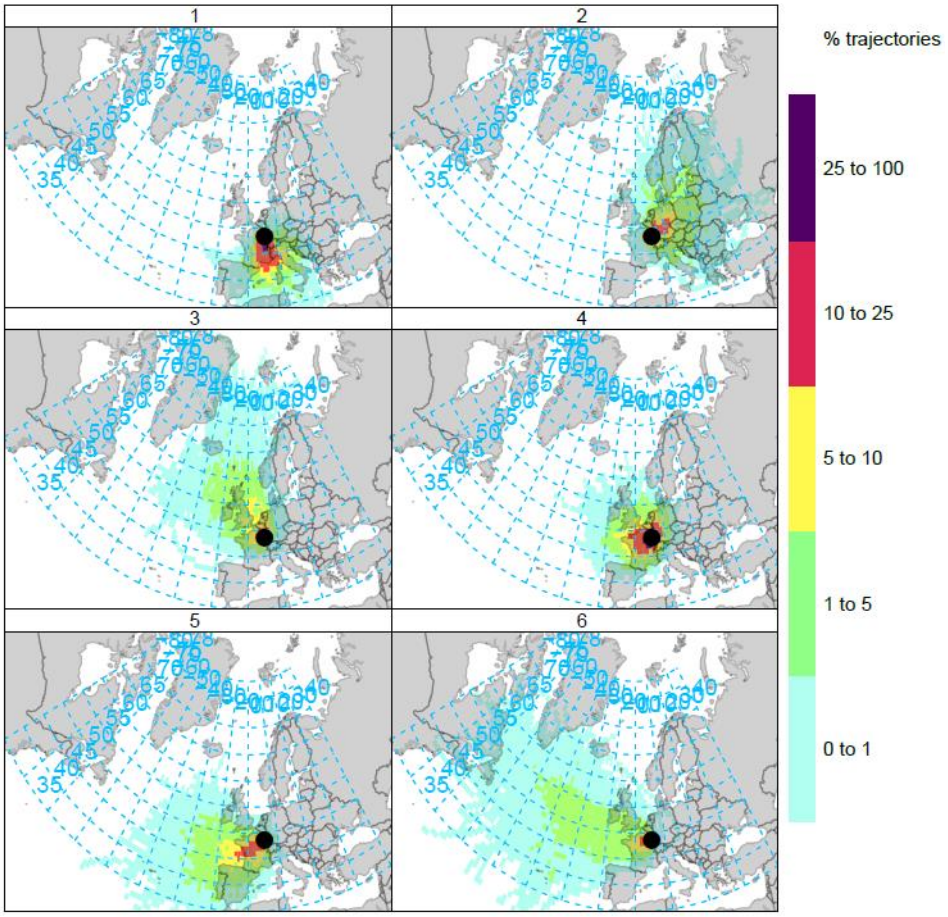

Figure 2: 96h back-trajectory frequencies reaching the OPE station top level for each of the 6 clusters identified using the HYSPLIT tools and the NCEP reanalysis for the period 2011-2018.

96h back trajectories were computed for the OPE station top level (120m) using the NCEP reanalysis fields and HYSPLIT model every 6 hours. As we focus on the afternoon mean residuals (defined as the differences between midday observations

and a smooth fitted curve), we only use back-trajectories reaching the OPE station at 12:00 UTC. The clustering tools from HYSPLIT were used to determine the main air masses type reaching the station. Based on the total spatial variance (TSV) metric, describing the sum of the within cluster variance, the optimal number of clusters was six (lowest number with a small TSV). The TSV plot is shown in Figure S1 of the supplementary material. The six clusters were defined as shown in Figure 2. This figure shows the frequency of trajectories for each cluster passing through the corresponding grid point and reaching the OPE station at 12:00 UTC. Clusters 1 to 3 are characterized by continental air masses. Cluster 4 is dominated by slow moving trajectories from the west. Cluster 5 and 6 are dominated by western marine trajectories.

2.3 GHG measurements system

The GHG measurement system was setup in 2011 with support from the ICOS Preparatory Phase projects. It was built in order to comply with the Atmospheric Station class 1 stations specifications from ICOS. It relies on a fully automated samples distribution system with remote control backed up by an independent robust spare distribution system. It includes several continuous analysers for the main GHG CO_2, CH_4 and N_2O, a manual flask sampler as well as specific analysers or samplers for tracers such as radon, CO and $^{14}CO_2$.

The continuous GHG measurement system is made of three main parts: an ambient air sample preparation and distribution component, a reference gases distribution component and a master component which conducts the main analysis sequence and controls the distribution and analysis systems through pressure and flowrate meters. The station flow diagram is described in Figure 3. The ambient air is collected on the tower at 10m, 50m and 120m levels and brought down to the shelter located at the tower base using 0.5 inches outer diameter Dekabon tubes equipped with a stainless steel inlet designed to keep out precipitations. Five sampling lines are installed at 120m,and three are installed at 10m and 50m. From the 120m level, one line is connected to the $^{14}CO_2$ sampler built by the Heidelberg University. Another sampling line is used to collect weekly flask samples. The continuous GHG measurements are performed using two independent sampling lines. The last line is a spare line which can be operated in case of trouble on one line or in case of temporary additional experiments such as independent audits as the ones performed in 2011 and 2014. At 10m and 50m, two lines are used for the continuous GHG measurement system. Another spare line is also installed for each of the 10m and 50m levels.

At each level, the continuous GHG monitoring system air is flushed from the tower using three Neuberger N815KNE flushing pumps (15 LPM nominal flow rate) and cleaned by two 40 micron and 7 micron Swagelok stainless steel filters. From each sampling line, a secondary KNF N86KTE-K pump (5.5 LPM nominal flow rate) is used to sample and pressurize the air (through a 2 micron Swagelok filter) to be dried and then analysed. A flowmeter is used to monitor the air flow in the flushing line and a pressure sensor is used to monitor the sampling line pressure. The air sample is pre-dried by a fridge through a coil (to increase the path in the fridge and the residence time). To further dry the sample, the air passes through a 335mL glass trap cooled in an ethanol bath at -50°C using a dewar. Once dried in the cryo water traps (-40°C dew point), the air sample is pressure regulated (~1150 hPa abs at the instrument inlet) and carried to the analysers.

The ambient air distribution component is driven by a control/command component, designed around a Programmable Logic Controller (PLC), which is dedicated to the selection and distribution of the ambient air sample from the three sampling heights. This distribution component selects an ambient air sample from one of the three levels using three 3-ways solenoid valves and then carry it to the drying system and to the analysers. Once analysed, the air sample flows back to the distribution panel where a backward pressure regulator controls the air pressure in the sample line. A pressure sensor monitors the pressure at the analyser inlets and a flow meter monitors the flow rate at the analyser outlets.

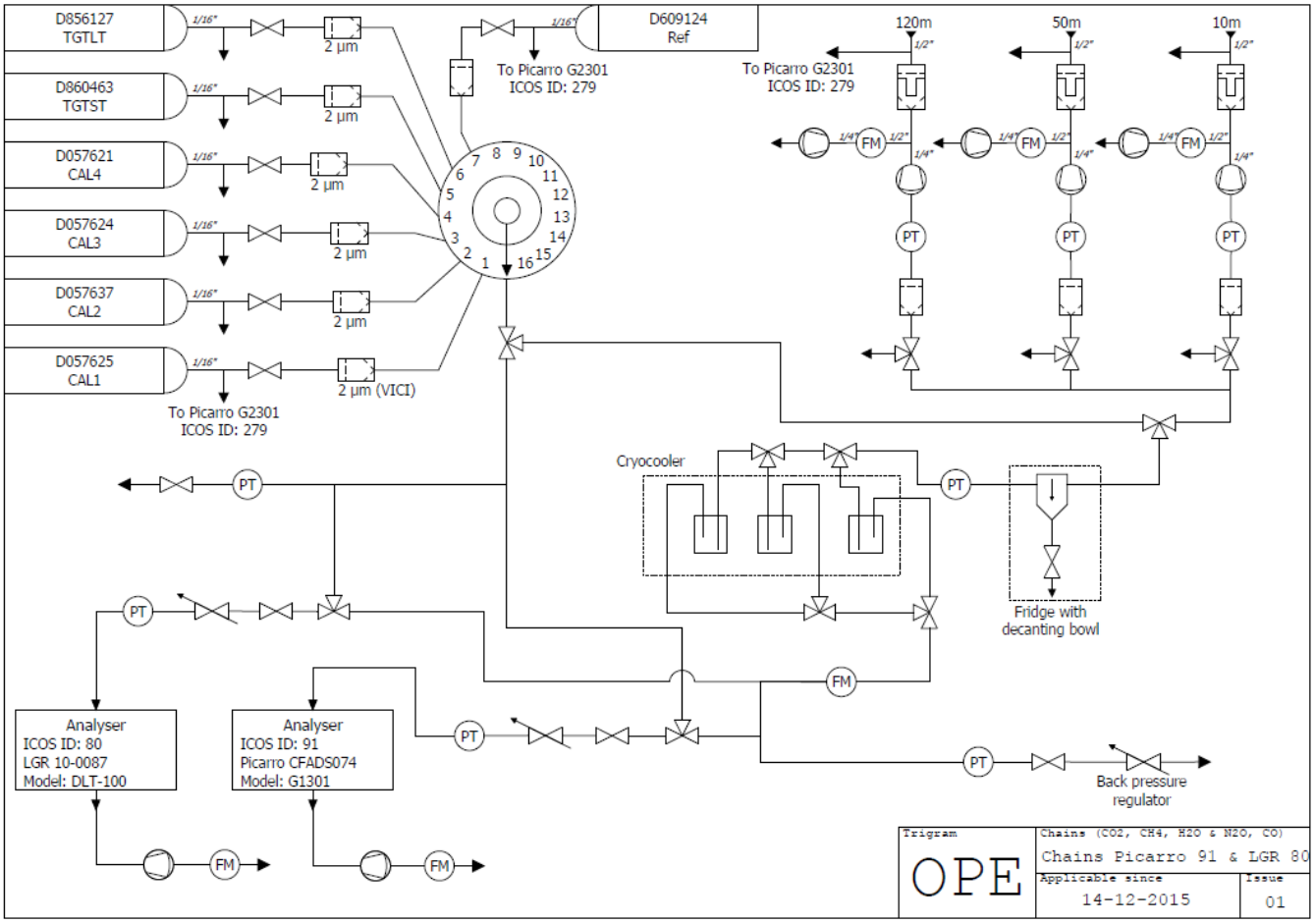

Figure 3: Flow diagram of the OPE GHG measurement system

The control/command component system selects between standards and ambient air, following the PLC's order, as it is responsible for the sequence management and quality control processes. The standard gas distribution component is based on a 16 position Vici Valco valve from which nine ports are connected to the analysers. The pressure of the selected standard gas or the ambient air sample is adjusted at the analyser inlet by a manual pressure regulator. All the1/8 or 1/4 inches stainless

steel distributing tubings are over pressurized to avoid any leakage artefact. According to ICOS internal rules, comprehensive leak checks are performed on a yearly basis and after all maintenance operations.

The analysers used are Picarro series G1000 and G2000 cavity ring down spectrometers (CRDS) for CO_2, CH_4, H_2O and CO and Los Gatos Research Off-Axis-ICOS-spectrometers for N_2O and CO. Each analyser used at the station first went through extensive lab tests at LSCE during the development of the ICOS Metrology lab at ATC (Lebegue et al., 2016, Yver Kwok et al., 2015). These initial tests provide valuable information about the intrinsic properties of the analysers, their precision, stability, water vapour sensitivity and temperature dependence.

Over the 2011-2018 period, the reference analysers were a Picarro G1301 (ICOS #91) which performs CO_2 and CH_4 (and H_2O) mole fractions analysis and a Los Gatos Research DLT100 (ICOS #80) which is used for CO (and H_2O) mole fraction measurement. A couple of spare and parallel instruments have been running either on the principal distribution system and /or on the spare distribution system following the same calibration and quality control strategy.

The routine operating sequence includes:

- Start with a complete calibration of four cycles of four standards lasting 8 hours followed by 30min of Long Term target (LTT) and then by 30min of Shirt Term target (STT),
- 5 hours of ambient air in cycles of three steps of 20min for the 10m level, 50m level and then 120m level
- 20min of Reference gas (REF)
- 5 hours of ambient air in cycles of three steps of 20min of the 10m level, 50m level and then 120m level
- 20min of STT

During the first years of the ICOS preparatory phase, the calibrations were performed every two weeks. For gas consumption issue and after optimization tests, they are now performed every three weeks.

The routine sequence is summarised on the table S1 in the supplementary materials

The flushing and stabilisation periods for the standards are 10 minutes meaning that the first 10 minutes of data for each standards are rejected. The flushing and stabilisation period for the ambient air samples are 5 minutes meaning that the first 5 minutes of data for each ambient air levels are rejected (only 15min on the total 20minutes every hour are available).The raw data are then calibrated using the two or three weeks complete calibration and REF working standards following Hazan et al. (2016). Raw data (between 1s and 5s resolution) are aggregated to minutes and hourly averages. The results presented here are based on validated minute data from mid 2011 to end of 2018.

The calibrations strategy includes four consecutive cycles of the four calibration cylinders sampled for 30 minutes each, the full calibration lasts 8 hours. An archive reference standard gas nicknamed Long Term Target (LTT) is injected every two or three weeks for 30 minutes while a common archive reference standard gas nicknamed Short Term Target (STT) is injected for 20 minutes every 10 hours. Another short term working standard nicknamed Reference (REF) gas is also used every 10 hours to correct the short term variability. The concentrations of the standards were defined following ICOS specifications

(Laurent, 2017). The standard gases are supplied with a SCOTT Nickel-plated brass regulator from a 50l Luxfer Aluminium cylinder. Before March 2016, the standard and performance cylinders used were prepared by LSCE and were traceable to WMO scales (CO_2:WMOX2007, CH_4: WMOX2007, CO: WMO-CO-X2014, N_2O: WMOX2007). Since March 2016, the standard and performance cylinders used have been prepared by the CAL of ICOS and are traceable to WMO scales (CO2:WMOX2007, CH4: WMO-2004, CO: WMO-CO-X2014, N2O: NOAA-2006). Short Term Target and Reference cylinders are refilled every 6 month by the Central Analytical Laboratories of ICOS. All the measurements data presented here were recalibrated on these scales.

The raw data from the analysers as well as the distribution system monitoring parameters are transmitted to the ATC database on a daily basis. Data are then processed following Hazan et al. (2016) including a specific water vapour correction for the remaining humidity, as well as a station specific automatic flagging process. Data products are then generated so that data quality control can be done on a regular basis. Additionally manual flagging is performed by the station Principal Investigator (PI) on the raw data as well as on the hourly aggregated data.

Figure 4 gives an overview of the different GHG continuous analysers in operation at the OPE station and their respective time periods. Details on the start and end dates and additional informations regarding ancillary instrumentations are in the table S2 in the supplementary material.

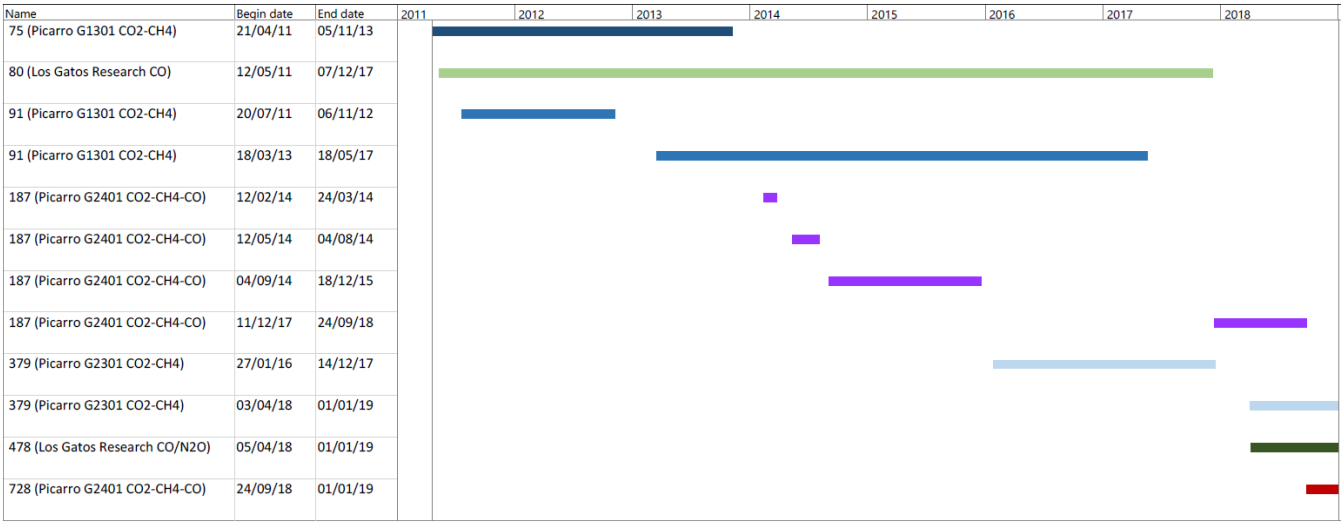

Figure 4: Time diagram showing the different GHG analysers operation at the OPE station.

2.4 Data processing

The GHG data cover several years and were collected using different sampling systems and analysers. In each of the individual time series, some data are missing because of either sampling issues, analysers problems or local contaminations near the station. Very local pollutions, for example due to field works or infrastructure maintenance, are very uncommon and occur only rarely. Power outage also happened because of lighting and construction work. Troubles on the sampling systems are

more frequent and include tube leaks, pump troubles, filters clogging or control/command component system failure. Analysers problems are also quite common and range from software issues, operating system failures, hardware problems (hard disk, fan, etc.), or worse, liquid contamination (from water or ethanol) of the optical cell.

Raw data from the instruments (mole fractions and internal parameters such as cell temperature/pressure, outlet valve), and from the air distribution system (sequence information and ancillary data such as pressure and flow rates in the sampling lines) are transferred at least once a day to the ATC data server. Data are then processed automatically as described in Hazan et al., (2016). Raw data are flagged using a set of parameters defined for each station and instrument. For the Picarro G1301 #91, G2301 #379 and G2401 # 728 analysers, the internal flagging parameters are the same as the ones shown on table 4 in Hazan et al. (2016). A manual flag is then applied by the station PI in order to eventually discard data using local station information (e.g. local contamination, maintenance operation, leakage, instrumental malfunctions, etc…). The list of descriptive flags available to the PI for valid or invalid data is shown in the table 2 of Hazan et al. (2016). The Table 1 presents the quantitative statistical summary of the status of the raw data for the different instruments used at the OPE station. Details of the internal flagging associated with the flags presented in this table can be found in the table 6 of Hazan et al. (2016). Between 62% and 72% of the raw data are valid while around 25% of the raw data are automatically rejected, 20% being rejected because of stabilisation/flushing. Corrections related to water vapour content and calibration are then applied. Finally, data are aggregated in time to produce minute, hourly and daily means.

Instrument	Compounds	Start	End	Flag	% raw data
75	CO_2/CH_4	21/04/2011	05/11/2013	O	72,1%
				N	25,80%
				K	2,10%
80	CO	12/05/2011	07/12/2017	O	71,0%
				N	23,5%
				K	5,50%
91	CO_2/CH_4	21/07/2011	22/06/2017	O	67,2%
				N	23,8%
				K	9,00%
187	CO_2/CH_4/CO	12/02/2014	03/04/2018	O	65,1%
				N	30,7%
				K	4,20%
379	CO_2/CH_4	27/01/2016	31/12/2018	O	71,7%
				N	24,9%
				K	3,40%
478	CO	27/01/2016	31/12/2018	O	62,4%
				N	24,9%
				K	12,70%
728	CO_2/CH_4/CO	27/01/2016	31/12/2018	O	65,6%
				N	25,0%
				K	9,40%

Table 1: Flags attributed to raw data from the different instruments between mid 2011 and end of 2018 2014. The last two columns provide the type of flag and the percentage of raw data that were attributed this flag. Flagged O data are valid data manually checked, while N and K flagged are non-valid data respectively automatically and manually rejected.

From these individual time series, we built three combined time series for CO_2, CH_4 and CO filling the gaps when possible The objective is to provide users with continuous time series, combining valid measurements in order to minimize the data gaps. Before the merging of the time series each instrument is quality controlled individually, and only measurements which are validated by the automatic data processing and the PI are considered for the combined dataset. For each measurement we

indicate the reference of the measuring instrument (unique identifier in the ICOS database), which gives the user the traceability of the analysers taken into account. To build these times series from various analyser datasets we used the priority order given in Table 2 for CO_2 and CH_4 and Table 3 for CO. The priority order is defined a-priori by the responsible of the station considering which analysers are fully dedicated to the station for long term monitoring purposes. In general secondary instruments are installed for shorter periods to perform specific additional experiments (like dry vs humid air samples, line tests, flushing flow rate tests, etc). For example, 91 was the main instrument for CO_2 and CH_4 followed by 379. While 91 was in maintenance, instruments 75 or 187 were used as spare instruments. At the beginning of 379 operation, 91 was still the main instrument, to keep the consistency of the time series as long as possible. When 91 operation stopped, 379 becomes the main instrument. When 379 was in repair the instrument 187 was used as spare instrument again. For CO the LGR analyser 80 was the main instrument followed by Picarro G2401 728. When the LGR 80 was out of order, we used either Picarro 187 or LGR 478 as spare instruments. In the case of the installation of two instruments for long-term measurements, then the priority order should take into consideration the performance of each one. It is the responsibility of the station manager to change the priority list in the ICOS database if needed. Merging the individual time series in such a way implies that the merged time series show steps in their uncertainties as individual analysers have different performance (see part 3 Data Quality Assesment for details about the steps in the repeatability performance).

Compound	Main analyzer	Spare analyzer	Start Date	End Date
CO_2 / CH_4		75 (Picarro G1301)	21/04/2011 00:00	20/07/2011 23:00
CO_2 / CH_4	91 (Picarro G1301)	75 (Picarro G1301)	21/07/2011 00:00	05/11/2013 23:00
CO_2 / CH_4	91 (Picarro G1301)	-	06/11/2013 00:00	11/02/2014 23:00
CO_2 / CH_4	91 (Picarro G1301)	187 (Picarro G2401)	12/02/2014 00:00	27/01/2016 00:00
CO_2 / CH_4	91 (Picarro G1301)	379 (Picarro G2301)	27/01/2016 00:00	22/06/2017 00:00
CO_2 / CH_4	379 (Picarro G2301)	-	22/06/2017 00:00	14/12/2017 00:00
CO_2 / CH_4		187 (Picarro G2401)	14/12/2017 00:00	03/04/2018 14:00
CO_2 / CH_4	379 (Picarro G2301)	-	03/04/2018 14:00	24/09/2018 14:30
CO_2 / CH_4	379 (Picarro G2301)	728 (Picarro G2401)	24/09/2018 14:30	-

Table 2: Order of priority (main vs spare analysers) for CO_2 and CH_4 with ICOS instrument identifiers and associated period

The different instruments were used in parallel for some time and it is thus possible to assess the systematic differences between the data for these common periods. The instruments may have shared sampling tubes, calibration and quality control gases but may have also used different air distribution system and different cylinders. Consequently, differences may occur due to problems associated with time synchronisation, air sampling (sampling and flushing pumps efficiency), calibration and water correction or any other causes not yet identified.

Compound	Main analyzer	Spare analyzer	Start Date	End Date
CO	80 (Los Gatos CO/N_2O)	-	12/05/2011 00:00	07/11/2012 00:00
CO	80 (Los Gatos CO/N_2O)	-	11/03/2013 00:00	12/02/2014 00:00
CO	80 (Los Gatos CO/N_2O)	187 (Picarro G2401)	12/02/2014 00:00	18/12/2015 00:00
CO	80 (Los Gatos CO/N_2O)	-	18/12/2015 00:00	07/12/2017 00:00
CO		187 (Picarro G2401)	14/12/2017 00:00	05/04/2018 18:00
CO	187 (Picarro G2401)	478 (Los Gatos CO/N_2O)	05/04/2018 18:00	24/09/2018 14:00
CO		478 (Los Gatos CO/N_2O)	24/09/2018 14:00	24/09/2018 14:30
CO	728 (Picarro G2401)	478 (Los Gatos CO/N_2O)	24/09/2018 14:30	-

Table 3: Order of priority (main vs spare analysers) for CO with ICOS instrument identifiers and associated period

Figure 5 shows the afternoon (12:00-17:00 UTC) hourly data difference between the different instruments analysing ambient air at 120m for CO_2 and CH_4. Large deviations in the afternoon means are revealed by such comparison. The summary statistics of the difference shown in Figure 5 for the 120m level (and for the 10m and 50m levels) are shown in the table S3 of the supplementary materials. On average over the full period the differences at 120m are -0.002 ppm for CO_2 and -0.27 ppb for CH_4, below the GAW/WMO compatibility goals (0.1ppm for CO_2 and 2ppb for CH_4). These significant deviations may come from various uncertainty sources, such as residence time difference in the sampling systems, water vapour correction, clock issue, or internal analyser uncertainties.

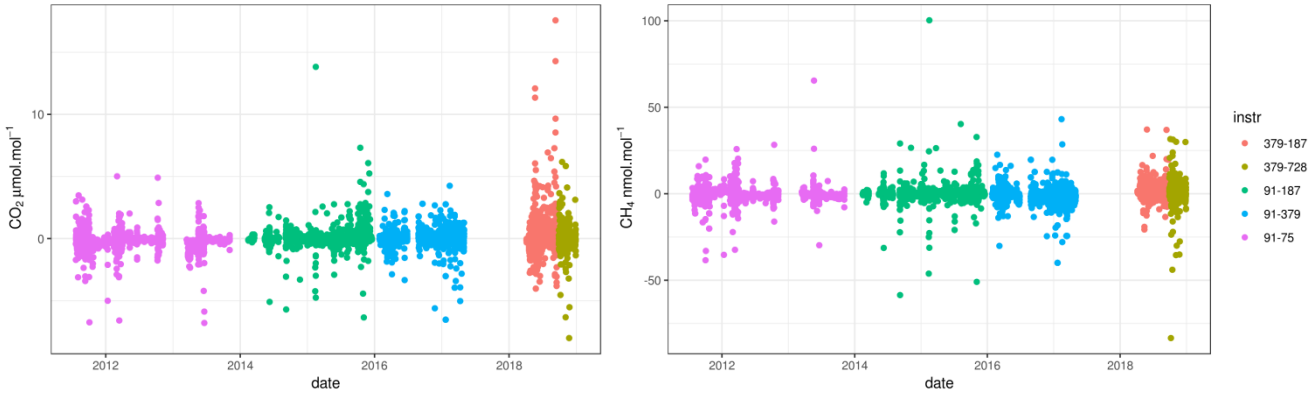

Figure 5: Difference between hourly mean afternoon (12:00-17:00 UTC) data at the top level 120m from the two instruments used at the same time at the OPE station from 2011 to 2018 for CO_2 (left panel) and CH_4 (right panel). The different instruments couples are shown in colour and their identifiers are labelled in the legend of the right panel.

No data filtering were applied regarding the differences and the overall biases are small (Table S3). Large differences can be observed on short periods, especially when the atmospheric signal shows very high variability. For such atmospheric conditions any difference in the time lag between air sampling and measurement in the analyser cell has a significant influence. The persistent presence of a bias between two instruments is used as an indication to perform checks on instruments and air intake

chains. For important differences, one of the instruments is generally disqualified based on the tests performed. In the case of moderate differences, the objective is to use this information for estimating uncertainties.

In a similar approach, Schibig et al. (2015) reported results from the comparison between CO_2 measurements from two continuous analysers run in parallel at the JFJ station in Switzerland. The hourly means of the two analysers showed a general good agreement, with mean differences on the order of 0.04 ppm (with a standard deviation of 0.40ppm). However significant deviations of several ppm were also found.

3. Data Quality Assessment

QA/QC protocols are applied at several steps of the measurements system. Every day, a conservative quality control is conducted from two complementary standpoints: First, the spectrometers intrinsic properties are verified, and secondly, the sampling system parameters are checked. On a weekly to monthly basis the field spectrometers performance are checked. A flask program also runs in parallel and is used to expand the atmospheric monitoring to other trace gases but also to assess the quality of the continuous measurements. Up to now, flask data were not fully available or were contaminated, and thus were not used in the present work. A complementary approach to assess compatibility uses round robin or so-called "cucumbers" cylinders circulated between stations within the ICOS European network. Finally, the station compatibility is also assessed during in situ audits using a mobile station and traveling instruments (Hammer et al, 2013; Zellweger et al., 2016).

In this section we used two metrics defined in Yver Kwok et al. (2015) for the quality control assessment of the data. These two metrics are usually calculated under measurement repeatability conditions where all conditions stay identical over a short period. The continuous measurement repeatability (CMR), sometimes called precision, is a repeatability measure applied to continuous measurements. The long-term repeatability (LTR), sometimes called reproducibility, is a repeatability measure over an extended period of time. As ICOS targets the WMO/GAW compatibility goals within its atmospheric network, the analysers must comply with the performance requirements specified in the Table 3 of the ICOS AS specifications report (Laurent 2017). ICOS precision limits of CO_2, CH_4 and CO measurements are set to respectively 50 ppb, 1 ppb and 2ppb. ICOS reproducibility limits of CO_2, CH_4 and CO measurements are set to respectively 50 ppb, 0.5 ppb and 1ppb.

3.1Short term target quality control: Field continuous measurement repeatability equivalent

In our basic measurement sequence, the air from a high-pressure cylinder (STT) is analysed twice a day with a ten hours frequency for at least 20 minutes to assess the daily performance of the spectrometers. This metric mainly describes the intrinsic performance of the spectrometers and not of the sampling system. It is a field estimation of the CMR and is computed as the standard deviations of the raw data over 1 min intervals, the first 10 minutes of each target gas injection being filtered out as stabilisation.

Figure 6 shows the monthly mean CMR of the combined time series of CO_2 and CH_4 using the same type of analysers. The time series of CO's CMR are shown in the supplementary materials (Figure S2). For CO_2, we observe a decrease of the CMR over the measurement periods, indicating an improvement of the instruments precision. Analyser #91 (Picarro G1301) was shipped to the manufacturer for a major repair including cell replacement between November 2012 and March 2013. The repair at the Picarro workshop improved the CMR performance of the analyser from above 0.06 to below 0.05 ppm. For this instrument, the factory estimated a CMR of 0.04 ppm in 2009 and the lab test at ATC MLab in 2012 estimated a CMR of 0.06 ppm.

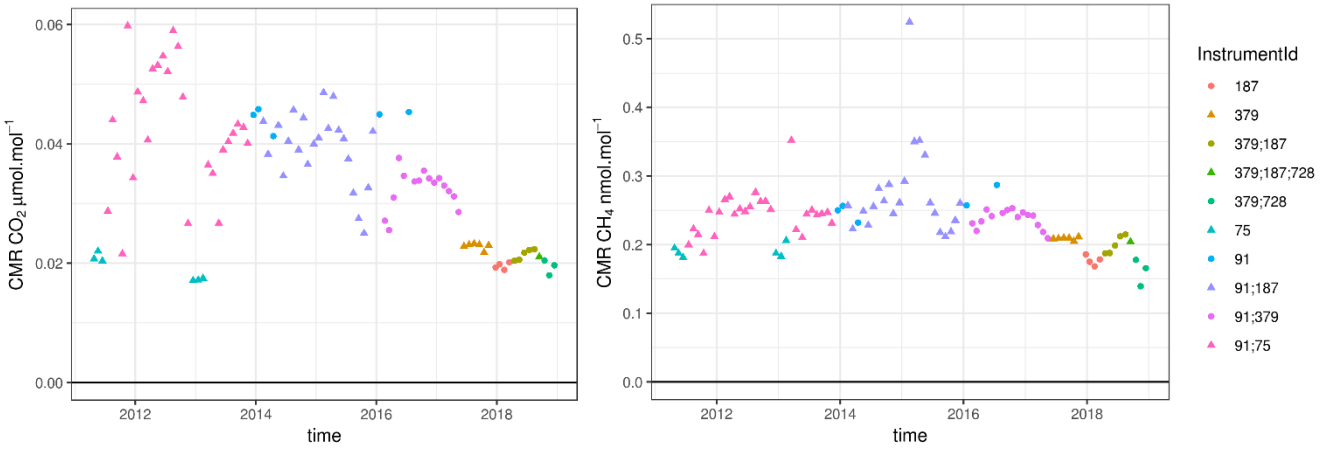

Figure 6: Monthly mean field Continuous Measurement Repeatability (CMR) for CO_2 (left panel), and CH_4 (right panel) estimated over time for the different instruments in operation at the OPE station over the 2011-2018 period. The different instruments are shown in color and their identifiers are labelled in the legend of the top and bottom panels. Some months, have several instruments running at the station and are identified with several labels

Using a gas chromatograph at the Trainou (TRN) tall tower, Schmidt et al. (2014) found a mean standard deviation in the hourly target gas injections of 0.14 ppm for CO_2, 3.2 ppb for CH_4 and 1.9 ppb for CO for the whole period of 2006-2013. Berhanu et al. (2016) presented their system performance using precision, a metric based on the standard deviation of the 1-min target gas measurements, at 0.05ppm for CO_2, 0.29ppb for CH_4 and 2.79ppb for CO using a Picarro G2400 spectrometer over 19 months from 2013 to 2014. Lopez et al. (2015) presented short term repeatability (a metric similar to CMR) estimates for the gas chromatograph system used at Puy de Dôme (PDD) at 0.1ppm for CO_2 and 1.2 ppb for CH_4, for the years 2010-2013. Ttable S4 of the supplementary materials summarizes these informations.

Table 4 presents the comparison of the CO_2 and CH_4 CMR for the instruments #75/91/187/379/728 estimated by the manufacturer, by the ICOS ATC MLab as well as the mean values from the station measurements over the 2011-2018 period. The station performance of each individual analyser is consistent with its performance estimated at the factory and at the ATC MLab. Performance is maintained over several years and was not disturbed by the station settings.

		CO_2 (ppm)			CH_4 (ppb)		
Analyser	**ICOS Id**	**factory CMR**	**ATC Mlab CMR**	**Field mean CMR**	**factory CMR**	**ATC Mlab CMR**	**Field mean CMR**
Picarro G1301	91	0.04	0.059	0.048	0.27	0.24	0.27
Picarro G1301	75	0.019	0.022	0.02	0.18	0.26	0.22
Picarro G2401	187	0.023	0.026	0.021	0.2	0.28	0,22
Picarro G2301	379	0.025	0.023	0.022	0.23	0.22	0.2
Picarro G2401	728	0.014	0.013	0.014	0.1	0.09	0.08

Table 4: Continuous measurement repeatability (CMR) estimated by the factory, MLab and field means over 2011-2018 of CO_2 (ppm) and CH_4 (ppb). Their model and ICOS Identifier are indicated in the first columns.

For CH_4, the factory estimated CMR for instrument #91 in 2009 was 0.27ppb and the initial lab tests at ATC MLab in 2012 estimated CMR for CH_4 at 0.24 ppb. The repair at the Picarro workshop did not modify the CMR performance of the analyser. For each instrument, the CH_4 performance is very stable over the years with very few outliers.

The CO performance (CMR and LTR) estimated at the station is compared to the factory and ATC MLab results in the Table 5.

		CO (ppb				
Analyser	**ICOS Id**	**factory CMR**	**ATC Mlab CMR**	**Field mean CMR**	**ATC Mlab LTR**	**Field mean LTR**
Los Gatos N_2O and CO	80	0.15	0.06	0.06	0.3	0.4
Picarro G2401	187	6.5	5.7	5.17	1.7	1.18
Los Gatos	478	0.06	0.09	0.05	0.09	0.05
Picarro G2401	728	2.7	2.69	2.76	0.22	0.33

Table 5: Continuous measurement repeatability (CMR) and long-term repeatability (LTR)) between factory, MLab and field mean over 2011-2018 of CO (ppb). Their model and ICOS Identifier are indicated in the first columns.

The CO CMR time series (Figure S2 of the supplementary materials) displays four different periods which are directly linked to the analysers used to build the merged time-series. We used two different analysers type: one built by Los Gatos Research (instruments #80 and #478) and one built by Picarro (instruments #187 and #728). These two types of analysers have very different internal properties as shown on table 5. The CO CMR results reflect such large difference (shown in Figure S2 of the supplementary materials), the CO CMR from Los Gatos Research instruments being much lower than the CO CMR from Picarro. The Picarro 187 and 728 CO LTR are significantly lower than their CO CMR. This means that their raw data have large high frequency variabilities but when averaged over several minutes these instruments are quite stable (they are not very sensitive to atmospheric or pressure changes).

Overall the precisions measured at the station for CO_2, CH_4 and CO remain similar to the initial values estimated by the manufacturer and the ATC laboratory, showing no degradation due to the design of the station or the measurement procedures.

3.2 Short term target quality control: Field long term repeatability

The field LTR is computed as the standard deviation of the averaged STT measurement intervals over 3 days as it is done during the initial test at the ICOS Metrology Lab. Data are then averaged every month. The same STT data are used but with a different perspective, more closely linked to the ambient air data uncertainty.

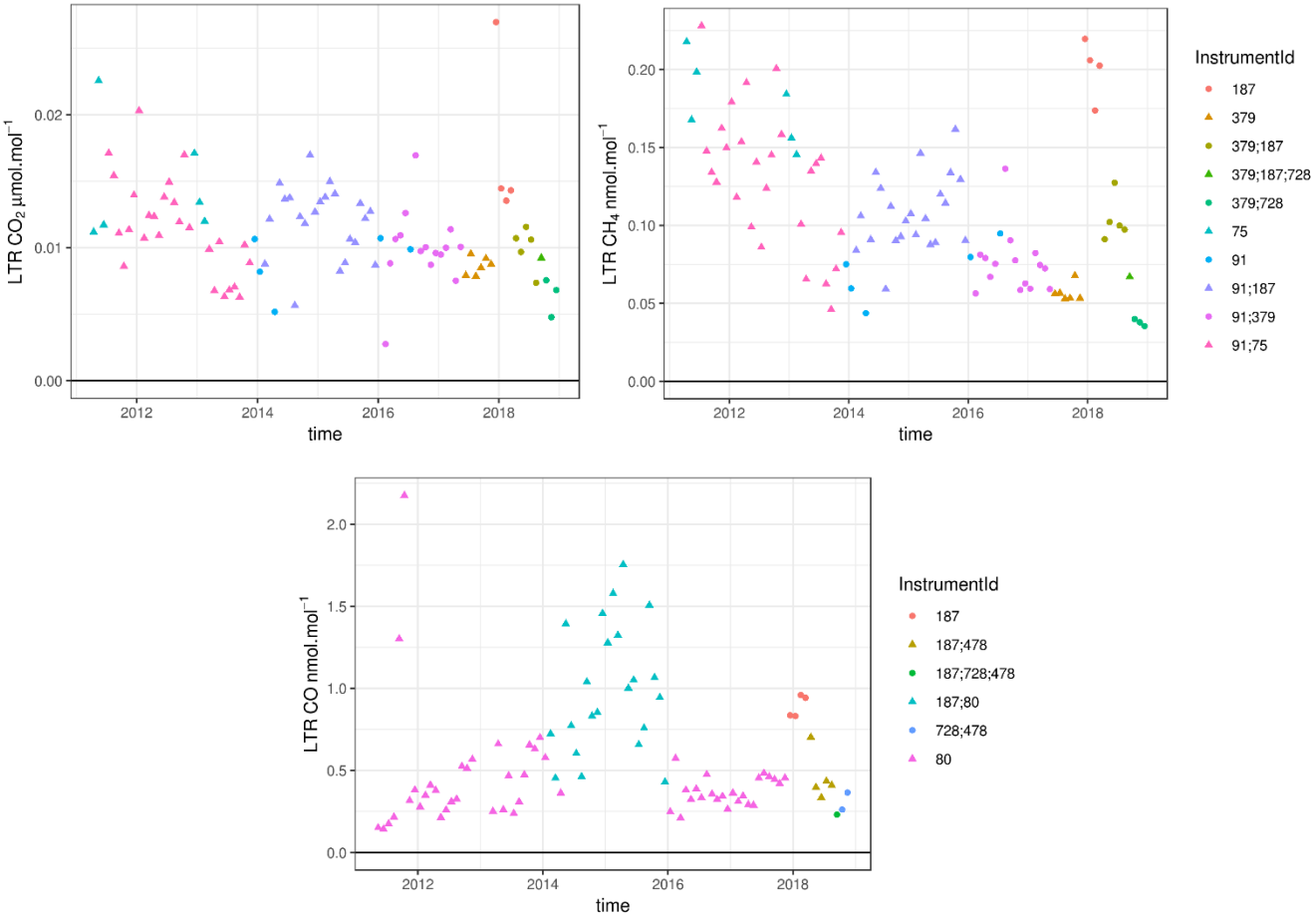

Figure 7: Monthly mean field long term repeatability (LTR) for CO_2 (top left panel), CH_4 (top right panel) and CO (bottom panel) estimated over time for the different instruments in operation at the OPE station over the 2011-2018 period. The different instruments are shown in color and their identifiers are labelled in the legend of the top and bottom panels. Some months, have several instruments running at the station and are identified with several labels

Figure 7 shows the monthly mean field LTR of the merged time series using the different instruments and sampling systems. This figure shows the uncertainties of the data related to the analysers (not the sampling systems). As for CMR, CO_2 and CH_4 LTR show decreasing trends suggesting an improvement of the internal performance of the spectrometers built by Picarro, of the air distribution system as well as data selection/flagging. The early part of 2018 experienced a clearly worse LTR compared to neighbouring months. This is mostly due to the use of the instrument #187, which has relatively poor performance compared to other instruments.

		CO_2 (ppm)		CH_4 (ppb)	
Analyser	ICOS Id	ATC Mlab LTR	Field mean LTR	ATC Mlab LTR	Field mean LTR
Picarro G1301	91	0.02	0.01	0.08	0.08
Picarro G1301	75	0.01	0.01	0.21	0.17
Picarro G2401	187	0.02	0.02	0.22	0.17
Picarro G2301	379	0.007	0.009	0.1	0.06
Picarro G2401	728	0.005	0.008	0.06	0.02

Table 6: Long term repeatability (LTR) of CO_2 (ppm) and CH_4 (ppb) estimated by MLab and field mean over 2011-2018. Their model and ICOS Identifier are indicated in the first columns

The comparison of the field mean LTR and ATC MLab LTR for the different instruments are shown in Table 6 for CO_2 and CH_4. The LTR field performance of the analysers are consistent with their initial assessments. Periods of lower CO_2/CH_4 LTR are associated with instruments #91, #379 or #728 while periods with higher CO_2/ CH_4 LTR are associated with instruments #75 or #187.

As for CMR, the CO LTR monthly time series shows four different periods but with a smaller contrast, associated with the type of analyser used at the station. Most periods with LGR instruments (#80 or #478) shows a LTR under 0.7ppb while periods with Picarro instrument #187 show a LTR above 0.5ppb.

Different periods have different uncertainty levels related to the instrument performance. While Los Gatos Research instruments show lower CO LTR they have stronger temperature sensitivities generating high short-term variability in conditions where the temperature is not well controlled. Corrections for these temperature induced biases required the frequent use of a working standard.

3.3 Station audit by traveling instruments

A metric such as CMR is very useful for monitoring the internal performance of instruments and for identifying any instrumental failure as early as possible. Other instrument related metrics such as calibration long term drift or calibration stability over the sequences are also useful for monitoring the instrument performance. However, they do not give an assessment of the overall measurement systems. Flask versus in-situ comparisons, or station audit by traveling instruments are recognized as essential tools in the performance and compatibility assessment of a measurement system. ICOS audits are performed by a mobile lab, hosted by the Finnish Meteorological Institute in Helsinki, and equipped with state of the art GHG analysers and traveling cylinders. The measurements data from the station are centrally processed at the ATC. However, the data produced by the Mobile Lab are computed separately to maintain the independent nature of the Mobile Lab and at the same time to evaluate the performance of the centralised data processing.

The OPE station was audited twice, once in summer 2011, soon after the station was set up, during the feasibility study of the travelling instrument methodology and then in summer 2014, when the ICOS Mobile Lab was ready for operation. During the two weeks intercomparison in 2011, significant differences for CO_2 and CH_4 were noticed between the FTIR traveling

instrument and the CRDS reference instrument (Hammer et al., 2013). As the two instruments have different temporal resolutions and different response times, the CRDS measurements were convoluted with an exponential smoothing kernel representing a 3 min turn-over time to match the FTIR specifications. For CO_2 the smoothed differences vary between 0.1 and 0.2 ppm with a median difference of 0.13 ppm and a scatter of the individual differences of approximately ±0.15 ppm. The smoothed CH_4 differences decrease from 0.7 ppb initially to 0.1 ppb, the median difference being 0.4 ppb. Such large differences were caused by relatively poor performances of the CRDS and FTIR instruments because of specific hardware problems but also related to the large temperature variations (10 K) within the measurements container. During the summer of 2011, the travelling instrument was also set up at the Cabauw (CBW) station in the Netherlands. The audit showed better instrument performance but the same kind of differences for ambient air comparisons. While the CO_2 deviations at CBW were partly explained by a travelling instrument intake line drawback and by calibration issues on the main measurement system, at OPE no final explanation has been found for the observed differences.

In the summer of 2014, the two months audit was performed using a Picarro G2401 travelling instrument as well as a FTIR. However the FTIR performance was not yet optimized and the difference in time resolution made it difficult to use it properly. Results from this instrument are not considered here. On average, the OPE standard cylinders analysed by the travelling instrument showed 0.03 ppm and 0.10 ppm higher CO_2 concentrations in the beginning and in the end of the audit, respectively, than the assigned values used to calibrate measurements at OPE. Similar results were found for CH_4 with relatively low differences ranging between 0 and 1 ppb. The instruments as well as the working standards (OPE and travelling standards) were calibrated against two different sets of standards, introducing biases in the measurements of cylinders but also of ambient air. The intercomparison was complicated by the fact that the station was struck by lightning three times during the summer, creating major power outage and electrical damages to the infrastructures. Such power outages generate shifts in the CRDS analyser response that prevent drift correction of the calibration response, degrading the analyser performance. The ambient air comparison was based on two sampling lines, one line supplying a dried Picarro G1301 (#91) and a wet Picarro G2401 (#187), and one independent line for the audit supplying the wet travelling instrument. The wet OPE G2401 data were corrected for water vapour by the factory Picarro correction, but the travelling instrument was corrected by an improved water correction based on water droplet test performed at the beginning of the intercomparison and using a simplified version of Method #2-EMPA implementation presented in Rella et al. (2013). The ambient air mole fractions for CO_2 by both dried and wet OPE analysers showed lower concentrations compared to the wet travelling instrument, by 0.10 ppm at the beginning of the audit, and 0.13 ppm at the end. Most of the differences in ambient air measurements can be explained by the bias in the reference scales.

When averaged over the whole period the OPE minus travelling instrument differences remain within the WMO/GAW component compatibility goal. The dried Picarro G1301 #91 measurements deviated on average by -0.05 ppm compared to the wet Picarro G2401 travelling instrument in the case of CO_2, and by 0.70 ppb in the case of CH_4. Similarly the wet Picarro G2401 #187 differs from the travelling instrument by -0.03 ppm and 1.80 ppb for CO_2 and CH_4, respectively. The CO

comparison was carried out for OPE-LGR and OPE-G2401 instruments and compared to the travelling instrument G2401: the average deviations were either higher than or barely within the WMO/GAW component compatibility goal (±2 ppb).

Vardag et al. (2014) presented similar intercomparison results at MHD over two months in spring 2013. For CO_2, the difference between the travelling instrument and the station analyser (Picarro G1301) for ambient air measurements at MHD was 0.14±0.04ppm. During this intercomparison there were no scale issues as the same scale was used on both system. However there could also have been a bias in the water correction effect. Still, most of the differences between the station data and the travelling instruments during the ambient air measurements remained unexplained. These results as well as the previously published results highlight the major difficulties that station PIs are facing with intercomparison interpretation and understanding. Upcoming sampling line tests, which are mandatory in the ICOS network at least on a yearly basis, may help to understand if the sampling design introduces artefacts.

3.4 Travelling "cucumbers" cylinders and station target tank biases

At the beginning of the station operation, quality control tanks, or targets, were not systematically used or calibrated. Calibrated tanks were used systematically from 2015 as working standards in order to monitor biases.

In addition the station OPE took part in the CarboEurope " cucumber " program in the EURO2 loop at the end of 2014, as well as in the ICOS program which started in September 2017. The aims of such programs are to assess measurement compatibility and to quantify potential offsets in calibration scales within a network. The results of these two sequences of "cucumbers" intercomparison are shown in Figure 8 along with the biases estimated for the station quality control cylinders.

The biases estimated from the target tanks operated at the station and the blind cucumber intercomparison biases are consistent for all species. CO_2 biases are found between -0.1ppm and 0.1ppm for most of the times except some outliers that still need to be understood. A slight trend may be present in the LTT CO_2 biases between 2014 and 2018. The STT results may show a trend as well but step changes are also present. We attribute the CO_2 biases signal to the convolution of step changes and interannual trend. The step changes may be due to cylinders changes. This possible CO_2 trend shown by the LTT (on the order of +0.02 ppm) remains unexplained at this stage. The re-evaluation of the CO_2 concentrations of calibration tanks at ICOS central facility could show a drift in their values, which would lead to a correction of the time series.

CH_4 biases are between -0.75ppb and 0.75ppb for most of the cases. CO biases show a large spread at the beginning of the station operation partly related to the temperature sensitivity of the Los Gatos Research analyser and the poor temperature control of the measurements container. Since 2016 the CO biases stay within the -5 ppb/+5 ppb range.

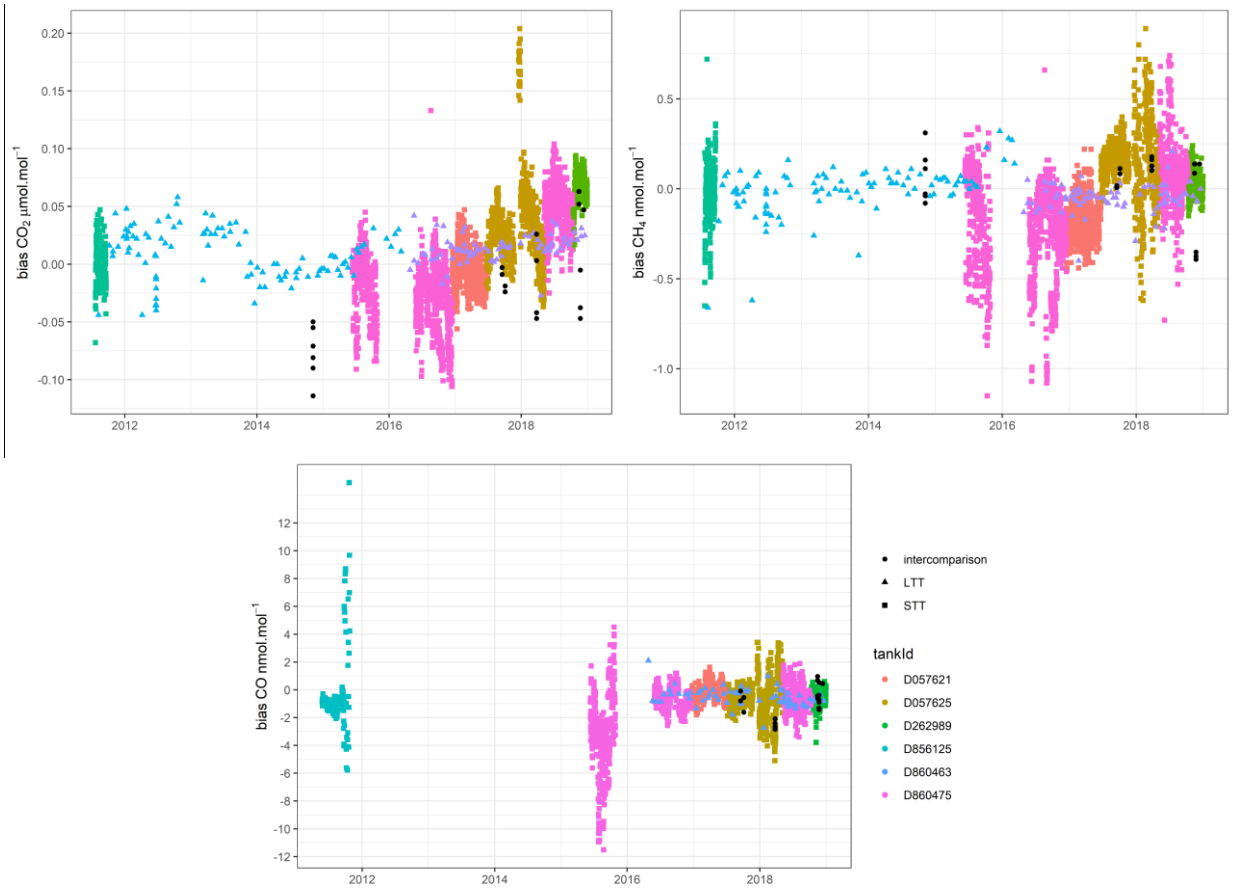

Figure 8 Target tanks biases over time for several tanks for CO_2 (top left panel), CH_4 (top right panel) and CO (bottom panel) in colours. The Short Term Target (STT) , Long Term Target (LTT) and "cucumbers" intercomparison biases are respectively shown in coloured squares, coloured triangles and black circle. The different colours are related to the different tanks used at the OPE station for quality control.

4. Results

Tall tower GHG concentration time series over mid latitudes continental areas exhibit strong variations from hours to weeks, seasonal and interannual time scales and even longer. Such variabilities are linked to local, regional and global meteorological variations, as well as land biosphere processes and human activities. We will first show the general characteristics of the time series. We will then analyse and show the diurnal cycles computed from the despiked hourly data. We will select only stable situations with low fast variability to focus on the regional scale and compute afternoon means for CO_2, CH_4, CO at the three sampling levels. The seasonal cycles and long-term trend will then be analysed and presented.

4.1 General characteristics of the CO_2, CH_4, and CO times series

Figure 9 shows the general characteristics of the afternoon mean mole fractions for CO_2, CH_4, CO at the OPE station at 10m, 50m and 120 m above ground level.

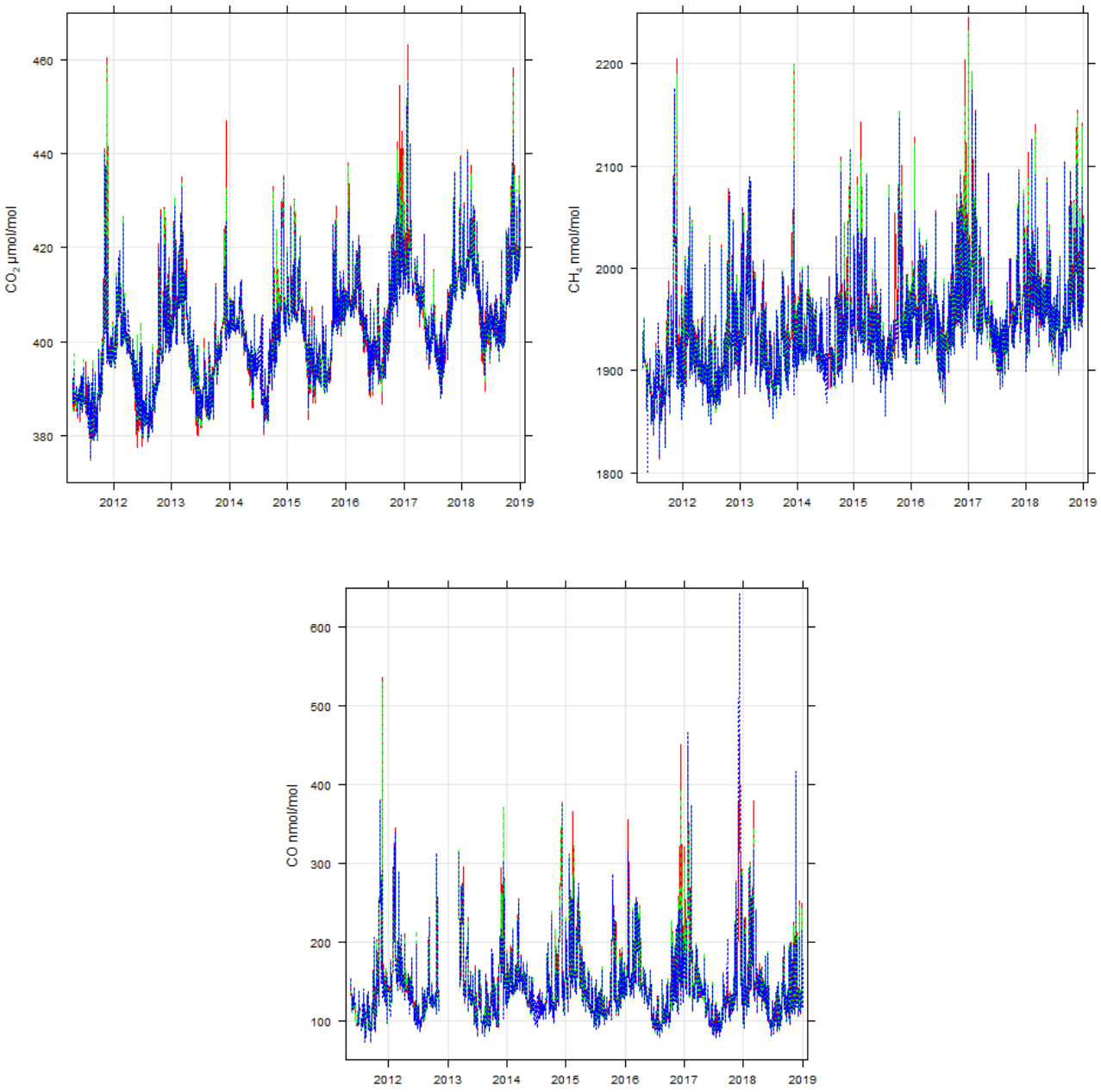

Figure 9: Afternoon (12:00-17:00 UTC) mean CO_2 (top left panel), CH_4 (top right panel) and CO (bottom panel) mole fractions measured at OPE station at 10m (red), 50m (green) and 120m (blue).

From the summer of 2011 to the end of 2018, the afternoon mean CO_2 at 120m varied from 375 ppm to a maximum of 455 ppm. Over this seven years period, the afternoon mean time series show synoptic variations as well seasonal variations and interannual trends. Similar patterns were observed at several other long term monitoring stations in western Europe over different periods (Popa et al., 2010, Vermeulen et al., 2011, Schmidt et al., 2014, Lopez et al., 2014, Schibig et al., 2015, Satar et al., 2016, Stanley et al., 2018, Yuan et al., 2019). At European background stations such as MHD coastal station or mountain stations (JFJ, Zugspitze ZUG or PDD) the interannual times series are dominated by long-term trends and seasonal changes. At regional continental stations (CBW, TRN or Bialystok BIK), the synoptic variations have a much larger intensity due to the proximity of the strong continental sources. The patterns and amplitude of synoptic variations and of seasonal changes also depend on the sampling height. The lowest level (10m) had a higher variability than the highest level (120m). At 10m, the summer minimum concentrations are lower than the 120m concentrations while the winter maximum concentrations are above the 120m concentrations. Vertical gradients of CO_2 are present year round but are stronger in summer and weaker in winter, and the gradient variability is much stronger in summer.

The CH_4 afternoon mean mole fractions time series are also characterized by a long-term trend with a weaker seasonal cycle. Synoptic variations could be as high as 150 to 200 ppb on hourly time scales and are stronger at the lowest level. Vertical gradients of CH_4 are present year round and show a small seasonal cycle. The CO afternoon mean mole fractions time series do not show any long-term trend but are characterized by strong seasonal cycles. Synoptic variations could be as high as 200 ppb on hourly time scales and are stronger at the lowest level. Vertical gradients of CO are much stronger in winter and weaker in summer. The CO lifetime in the atmosphere is strongly related to OH radicals, the major sink, which changes from season to season. During summer, the combined effects of a more active sink, weaker « local » sources and a strong vertical mixing lead to lower concentrations, with less variability and weaker vertical gradients. In winter, the OH sink efficiency decreases, local sources are stronger and the meteorological conditions favour non-dispersive situations and weaker vertical mixing leading to higher CO concentrations and stronger vertical gradients.

4.2 Diurnal Cycles and vertical gradients

The diurnal cycles of trace gases result from atmospheric dynamics (especially the daily amplitude of the boundary layer height), surface fluxes and atmospheric chemistry. The mean diurnal cycles of CO_2, CH_4 and CO are shown in Figure 10 for the three sampling levels (10m, 50m and 120m). Despiked hourly data (not detrended nor deseasonalized) were used to compute the mean diurnal cycles. CO_2, CH_4 and CO mole fractions displays similar diurnal cycles because of the similar atmospheric dynamics control: large increase of mean mole fractions and vertical gradients during night time in opposition with a reduction of mean mole fractions and vertical gradients during daytime. During the afternoon, while the lowest level CH_4 and CO mole fractions stay larger than at the top level, CO_2 mole fraction at the lowest level are slightly lower than at higher level. This CO_2 depletion is due to the vegetation growth and photosynthesis (which are stronger in summer and almost disappearing in winter).

Lags are noticeable between the different levels in the CO_2 and CH_4 diurnal cycle. The night-time peak concentrations occur earlier at the lowest level followed by the intermediate level and then followed by the highest level. The daytime minimum seems to be reached at the same time at the three levels. Then the late afternoon increase is much faster at the lowest level and is also delayed at the highest level. The diurnal cycles of CO_2 and CH_4 are larger in spring and summer while for CO it is larger in winter.

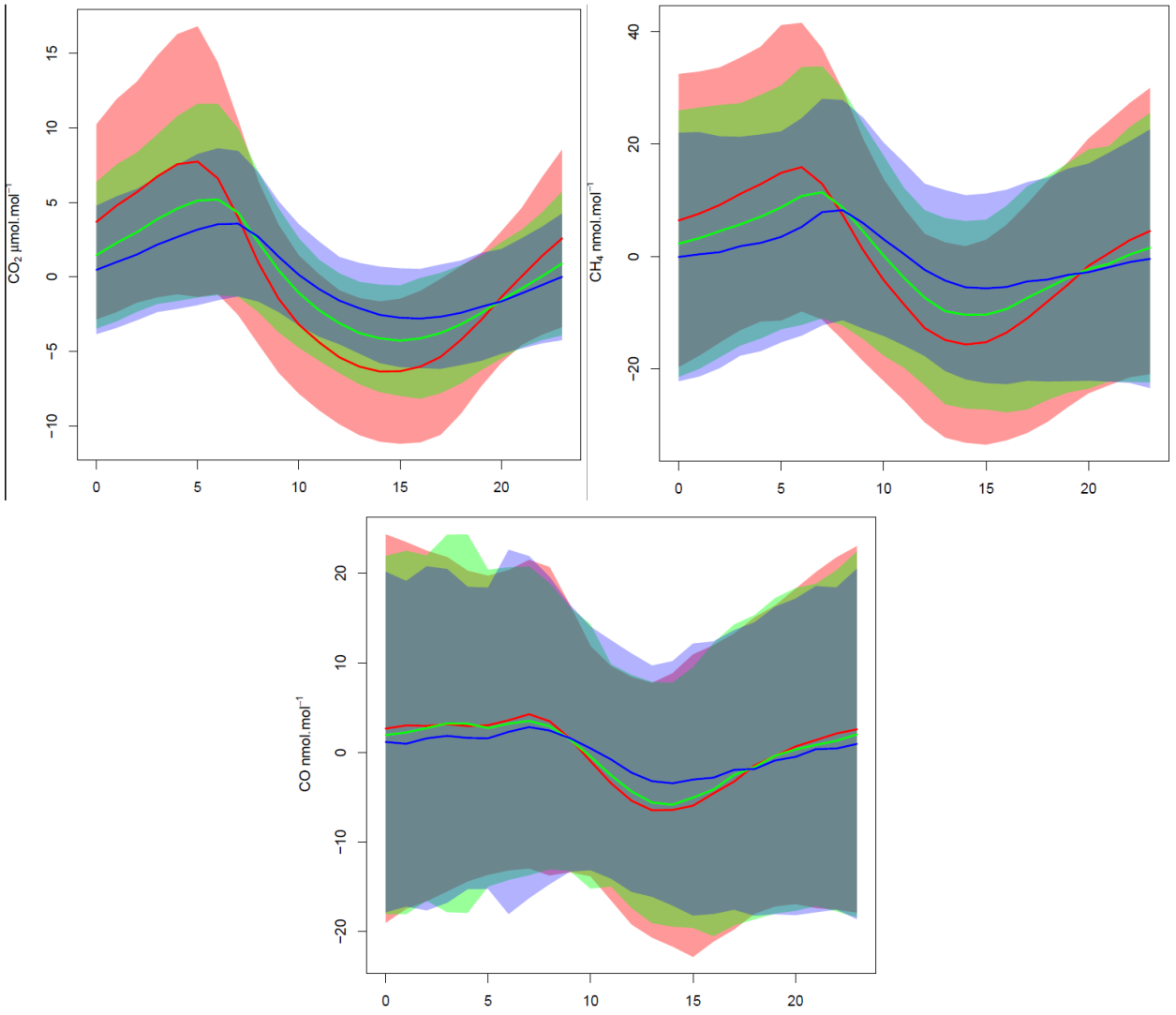

Figure 10 Mean diurnal cycles of CO_2 (top left panel), CH_4 (top right panel) and CO (bottom panel) for the three sampling levels 10m (red), 50m (green) and 120m (blue), computed over the period 2011-2018. The shaded area correspond to the + and – 1 standard deviations around the mean diurnal cycles.

For the three compounds, the vertical gradients are much stronger at night, and the highest concentrations are measured near to the ground. During the day, the gradients almost disappear, due to the vertical mixing of the low atmosphere. In spring and summer, the lowest level CO_2 afternoon concentration is slightly below the highest level reflecting the photosynthesis pumping of CO_2 by the plants. Vertical gradients build up again in the late afternoon. For CH_4 and CO the vertical gradient stays the same all along the day, the lowest level being higher than the highest levels.

In the warm period (from May to September) the mean vertical gradient of CO_2 is 0.4ppm during the afternoon (12:00-17:00 UTC) and -9.95ppm at night (00:00-05:00 UTC). During the cold period (from October to April) the mean vertical gradient of CO_2 is -0.24ppm during the afternoon (12:00-17:00 UTC) and -3.5ppm at night (00:00-05:00 UTC). Similar patterns were observed at CBW, for the 1992 -2010, period but with stronger amplitude (Vermeulen et al., 2011). In winter, the lower levels always show the highest CO_2 concentrations, and the mean vertical gradient is between 4ppm (daytime) and 10ppm (night-time). In summer, the vertical gradients of CO_2 were also very small during the afternoon and show net uptake of CO_2 at the lowest level (between 0.5 and 1 ppm). Night-time summer gradients were largest in summer and autumn, peaking at 04:00 UTC around -30ppm. Satar et al. (2016) showed vertical gradients of GHG concentration at the Beromunster station. In June 2013, the vertical gradients of CO_2 were negative between 18:00 UTC and 06:00 UTC reaching around -10ppm at 3:00 UTC while they were positive between 09:00 and 15:00 UTC with an amplitude of 1 to 3 ppm. In January 2013, the vertical gradients stay the same (negative) all along the day with amplitudes between -5ppm and -10ppm. Stanley et al. (2018) showed the vertical gradients of CO_2 and CH_4 mole fractions at two tall towers in the United Kingdom (UK). Daytime vertical differences of CO_2 were very small (<1ppm) (positive in winter and negative in the other seasons). Nigh-time vertical gradients of CO_2 were always negative between -3ppm and -8 ppm.

In the warm period the mean CH_4 vertical gradient is -0.5ppb during the afternoon (12:00-17:00 UTC) and -20.7ppb during the night (00:00-05:00 UTC). During the cold period (from October to April) the mean vertical gradient of CH_4 is -4 ppb during the afternoon and -18.5 ppb at night. Similar patterns and amplitudes were shown in the UK by Stanley et al. (2018). Vermeulen et al. (2011) also presented similar patterns but with larger amplitudes, the CBW vertical gradients of CH_4 reaching -300ppb during summer between the 20m and 200m levels.

4.3 Regional scale signal extraction

Our aim in this paper is to present the general behaviours of the major GHG at the station focusing on relatively large scale. The station hourly time series exhibit strong variability from hourly to interannual time scales. These variations may be related to meteorological and climate changes, and to sources and sinks variations. We are mostly interested in the regional signatures at scales that can be approached using model inversion and assimilation framework. For this reason we want to isolate the situations where the local influence is dominant and is shadowing the regional signature from the time series and data aggregation. We then need to define the background signal on top of which the regional scale signal is added.

Such local situations and background definitions may be extracted purely from time series analysis procedures, or may be constrained on a physical basis. The main difficulty is to correctly define the baseline signal of the measured time-series and

to adequately flag local spikes. El Yazidi et al. (2018) assessed the efficiency and robustness of three statistical spikes detection methods for CO_2 and CH_4 and concluded that the two automatic SD and REBS methods could be used after a proper parameters specification. We used the El Yazidi et al. (2018) method on the composite merged minute time series to filter out « spike » situations. From this despiked minute dataset we built hourly means, which were used to analyse the diurnal cycles. Focusing on data with regional footprints, we selected only afternoon data with low hourly variability when the boundary layer is larger and the vertical mixing is more. efficient We excluded data showing large variations by using the minute standard deviations. Hourly data with minute standard deviations larger than the three interquartile range computed month by month were excluded from the afternoon mean, leading to a rejection of 2.9 % to 4.2% of the hourly means of CO_2, CH_4 and CO.

We then used the CCGCRV curve fitting program from NOAA (Thoning et al., 1989) with the standard parameters set (npoly=3, nharm=4) to compute the mean seasonal cycles and trends for the three compounds. CCGCRV results were compared with similar analysis performed with the openair package (Carslaw and Ropkins, 2012) of R for the seasonal cycle and the trend using the Theil-Sen method (Sen, 1968). These seasonal cycle and trend components of the time series are dominated by large-scale processes. In addition strong intra-seasonal variabilities are observed that are related to local and regional scale factors. We then computed the afternoon mean residuals from the seasonal cycle and trends using CCGCRV results.

4.4 Seasonal cycles

Figure 11 shows the mean seasonal cycles of CO_2, CH_4 and CO at the three measurement levels (10m, 50m and 120m agl). Each of the three GHG displays a clear seasonal cycle, with higher amplitudes at the lower sampling levels. Minimum values are reached during summer when the boundary layer is higher and the vertical mixing is more efficient. In addition to the boundary layer dynamics, the seasonal cycle of the surface fluxes and the chemical atmospheric sink also play significant roles. The correlations of dynamic and flux processes at the seasonal scale make it difficult to distinguish the role of each process. CO_2 vertical gradients are observed in late fall - early winter when the CO_2 concentrations at 10m are larger than at 120m.

Minimum values are reached in late summer for CO_2, around the end of August with no vertical gradients around this minimum. Vertical gradients appear in late spring with a maximum gradient in June when a secondary minimum is observed at the lowest level but not at the higher levels. The amplitude of the CO_2 seasonal cycle is nearly 21ppm at the three levels. The CO_2 seasonal cycle amplitudes observed at BIK and CBW were between 25ppm and 30 ppm depending on the sampling height (Popa et al., 2010; Vermeulen et al., 2011). The two early and late summer CO_2 minima were also observed by Haszpra et al. (2015), at the Hegyhatsal tall tower in western Hungary between 2006 and 2009 and their timing are very close to OPE. But only one summer minimum between August and September was observed at the BIK (Popa et al., 2010), CBW (Vermeulen et al., 2011) and TRN tall towers (Schmidt et al., 2014) and at the JFJ, Schauinsland (SSL) or ZUG mountains stations (Yuan et al., 2019). Ecosystem CO_2 flux measurements operated in 2014 and 2015 near the OPE atmospheric station revealed that the forest and

grassland Net Ecosystem Exchange had two maxima in early summer and late summer with a decrease in between (Heid et al., 2018). The two early and late winter maxima were also observed by Popa et al. (2010) at the BIK tall tower with similar timings, end of November and February. But only one winter maxima was observed in January at CBW (Vermeulen et al., 2011), TRN (Schmidt et al., 2014) and Hegyhatsal (Haszpra et al., 2015), in February at SSL and in March at the JFJ or ZUG mountains stations (Yuan et al., 2019).

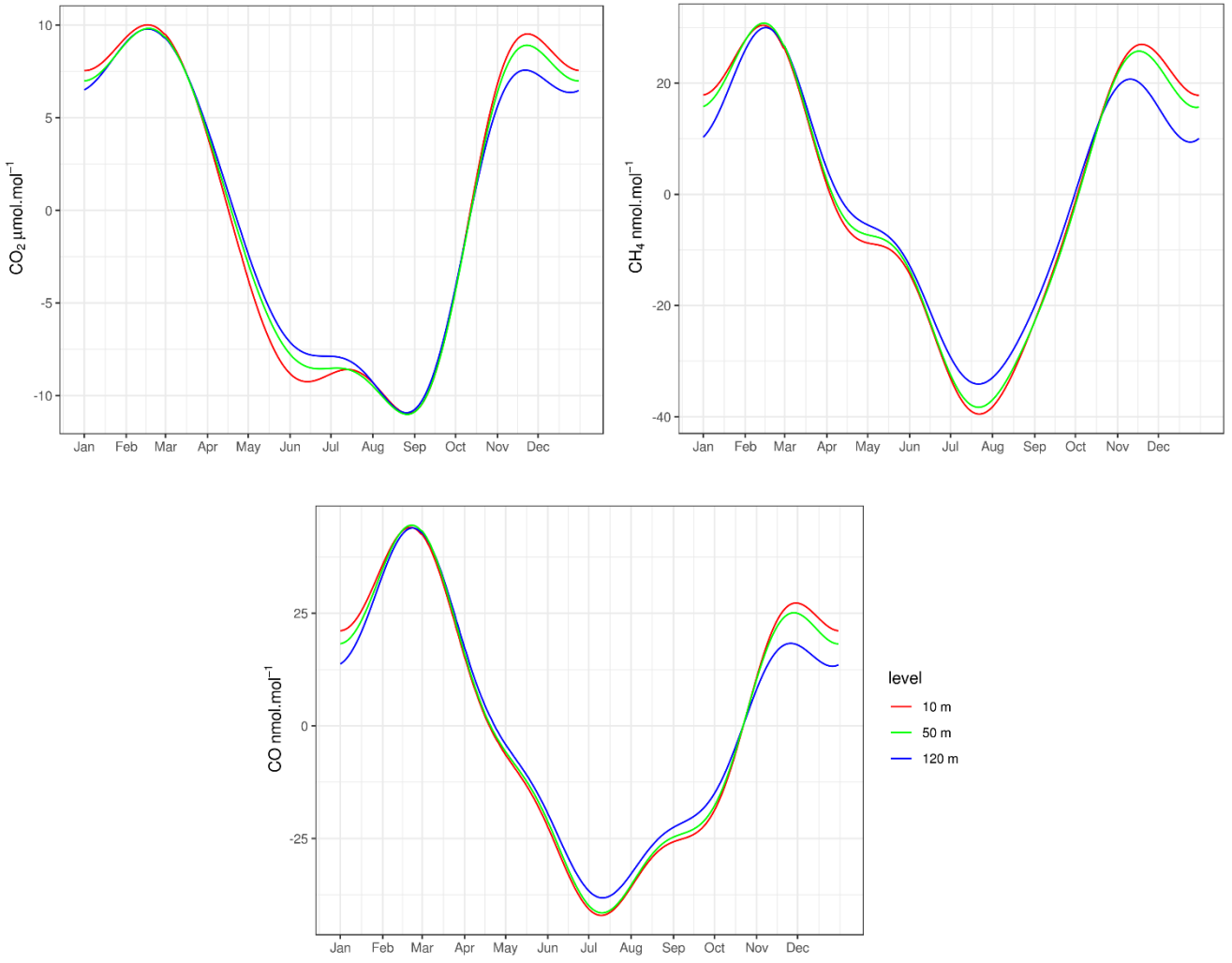

Figure 11:Mean seasonal cycles of the afternoon data at the three measurement levels (10m in red, 50m in green and 120m in blue) for CO_2 (top left panel), CH_4 (top right panel) and CO (bottom panel) computed over the 2011-2018 period using CCGCRV.

Minimum CH_4 values are observed in July and maximum values are reached in February and November. The peak-to-peak amplitude of the CH_4 seasonal cycle is nearly 70ppb at the three levels. The vertical gradients of CH_4 are stronger in mid-summer and early winter compared to the other seasons. At BIK, there was only one maximum in December and minimum values were reached between May and June (Popa et al., 2010). The seasonal cycle amplitude was between 64 and 88 ppb. At

CBW, CH_4 concentrations peaked at the end of December and were at minimum at the end of August. The seasonal cycle amplitude was between 50 ppb and 110 ppb (Vermeulen et al., 2011).

The CO seasonal cycle peaks at the end of February, with a secondary peak at the end of November. Minimum values are reached in July, earlier than the CO_2 and CH_4 minimum. The peak-to-peak amplitude of the CO seasonal cycle is between 80ppb and 90ppb. At BIK, the CO maximum was reached in January (with a delay compared to CO_2 and CH_4) and minimum values were observed in June, with a peak to peak seasonal cycle amplitude between 130ppb and 200ppb (Popa et al., 2010). At CBW, the CO maximum was reached in January (also with a delay compared to CO_2 and CH_4) and minimum values were observed in August. The peak to peak CO seasonal cycle amplitude varied between 90ppb and 130ppb (Vermeulen et al., 2011). At OPE, the vertical gradients of CO are highest in November and December. This highlights the enhanced winter anthropogenic emission probably associated with domestic heating as well as reduced atmospheric mixing. Large-scale transport may contribute to the increase as emission increases in winter on continental scale. However local activities also contribute as shown by the stronger vertical gradients and the higher mole fraction levels near the ground. CO_2 vertical gradients are stronger in November and December, as also shown in the CH_4 and CO vertical gradients, and are weaker from January to April.

4.5 Trends

Table 7 reports the mean atmospheric growth rates computed for the three compounds at the top level using CCGCRV and Theil-Sen approaches. The mean annual growth rate of CO_2 over the 2011-2018 period is 2.5 ppm/year using the Theil-Sen method and 2.3 ppm/year using CCGCRV. This is consistent with the Mauna Loa global station rate which is also 2.4 ppm/year on average for the period 2011-2018. It is stronger than the growth rate reported for ZUG mountain station: 1.8ppm /year, for 1981-2016 (Yuan et al., 2019), as well as CBW: 2.0 ppm/year, over 2005-2009 (Vermeulen et al., 2011). Such comparisons are only qualitative and must be used with caution, as the time period considered are different. However, they suggest that the atmospheric CO_2 growth may speed up in the European mid-latitudes

OPE-120m	CO_2 (ppm)	CH_4 (ppb)	CO (ppb)
CCGCRV 2011-2018	2.35 (1.93 ;2.77)	8.85 (7.35 ; 10.34)	-0.22 (-3.9 ; 3.5)
Theil-Sen2011-2018	2.54 (1.92 ; 3.28)	8.91 (7.64 ;9.96)	-0.49 (-1.71 ;0.73)

Table 7: Growth rates of CO_2, CH_4 and CO mole fractions at OPE 120m level for the period 2011-2018 computed on the afternoon mean data using the CCGCRV and Theil-Sen methods. 95% confidence intervals are displayed for each compound and method.

The mean annual growth rate of CH_4 over the 2011-2018 period is 8.8 ppb/year using CCGCRV and 8.9 ppb/year using the Theil-Sen method. It is slightly higher than the annual increase in Globally-Averaged Atmospheric Methane from NOAA

which is 7.5 ppb /year over the 2011-2017 period. A slightly decreasing non-significant trend is seen for CO at OPE over the 2011-2018 period. This finding is consistent with recent observations in Europe and in the US. After a long global decrease since the 1980's, the CO decrease has declined for several years after reaching values below 2 ppm (Lowry et al., 2016, Zellweger et al. 2016).

4.6 CO_2, CH_4 and CO residuals

We analysed the120m level residuals from the trend and seasonal cycle fitted curves with regard to air masses back-trajectories using the six clusters defined for the afternoon back trajectories (see Figure 2). Figure 12 shows the boxplots of the residuals for each month and back-trajectories cluster. The boxplot displays the first and third quartile and the median of the residuals as well as the overall data extension.

The residuals of the three compounds are significantly stronger in the cold months than during the warm months. Clusters 5 (shown in blue in Figure 12) and 6 (cyan) are associated with typical oceanic air masses with 96 h back-trajectories reaching far over the Atlantic Ocean. These air masses are associated with the lowest residuals variability (smallest boxplot extension). Negative residuals are noticed year-round for CH_4 and CO and during the cold months for CO_2 (positive during warm months). Clusters 1 (brown) and 2 (red) are associated with southern and eastern trajectories. The associated residuals are much stronger and show large variabilities among the different synoptic situations with potential large deviations from the background. Positive residuals are associated with Cluster 2 year-round for CH_4 and CO and during the cold months for CO_2. Cluster 3 (orange) is associated with either negative or positive residuals for the three compounds. Cluster 4 (green) is characterised by relatively "stagnant " air masses with back-trajectories that do not extend far from the station in any particular directions. This type of air masses is associated with high residuals variability for the three compounds during the cold months. The residuals can be either positive or negative and show large spreads among the situations.

cluster	**1**		**2**		**3**		**4**		**5**		**6**	
period	**warm**	**cold**	**warm**	**cold**	**warm**	**cold**	**warm**	**cold**	**warm**	**cold**	**warm**	**cold**
CO_2 / CH_4	0.21	0.92	0.33	0.89	0.01	0.84	0.47	0.86	0.18	0.8	0.24	0.87
CO_2 / CO	0.16	0.91	0.4	0.87	0.24	0.85	0.52	0.91	0.24	0.74	0.24	0.78
CH_4 / CO	0.74	0.93	0.87	0.84	0.71	0.87	0.76	0.92	0.75	0.85	0.78	0.88

Table 8 Correlation coefficients between the compounds residuals for each cluster, split between a warm period from April to September and a cold period from October to March.

Table 8 shows the correlation coefficients between the compounds residuals for each back-trajectory cluster, split between a warm period from April to September and a cold period from October to March. During the warm period, the correlation coefficients between CO_2 and either CH_4 or CO are low except for Cluster 4. However, the correlation coefficients between CH_4 and CO are around 0.75 for each cluster. During the cold period, the correlation coefficients between the different

compounds are high and significant for every type of back-trajectory. Similar seasonal pattern for the CO_2/CO residuals and CO/CH_4 residuals were shown by Satar et al. (2016) in their two years analysis of the Beromunster tower data in Switzerland.

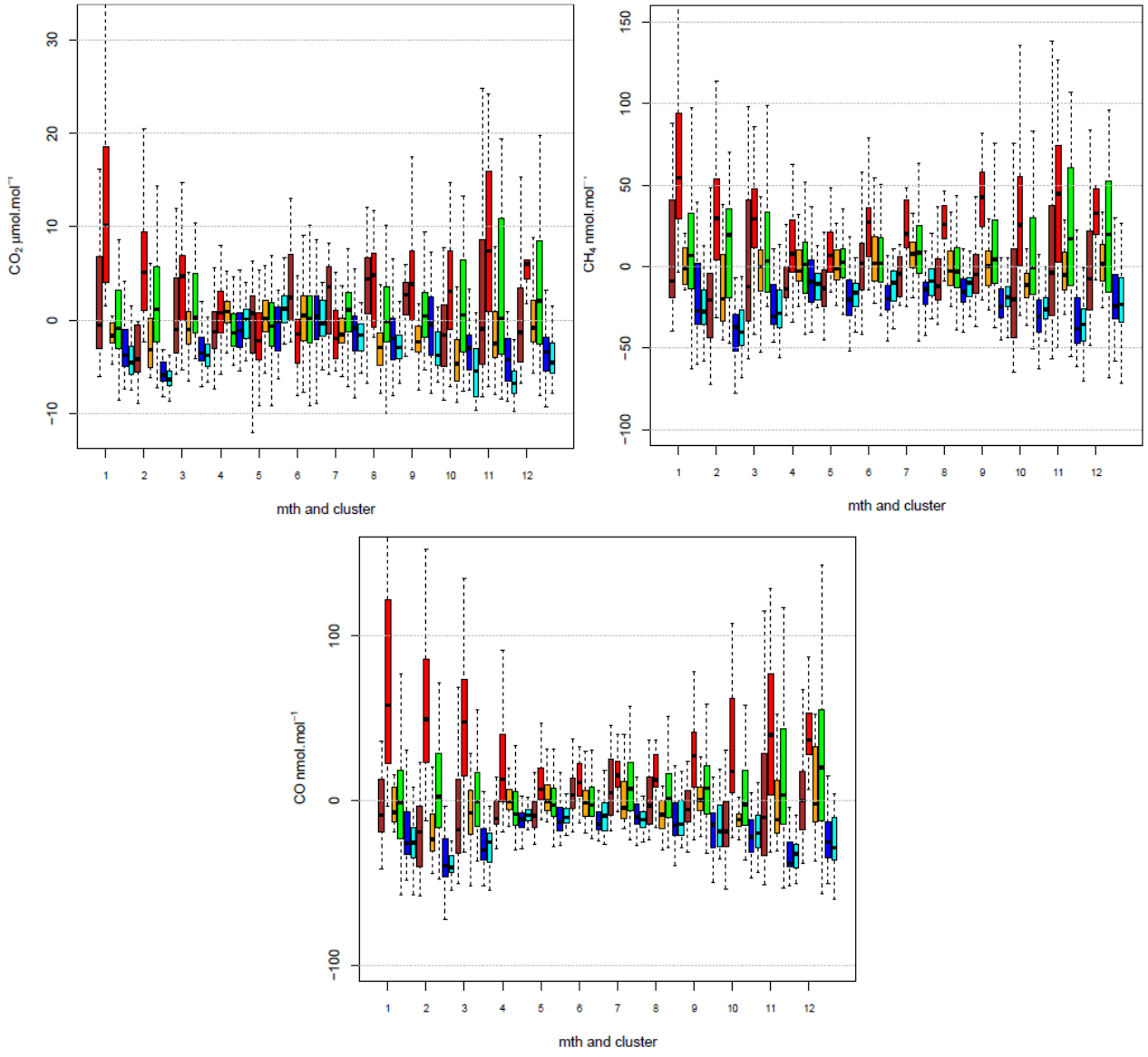

Figure 12: Seasonal boxplot of the CO_2 (top left panel), CH_4 (top right panel) and CO residuals (bottom panel) at OPE 120m levels by cluster occurrence (cluster 1: brown, cluster 2 : red, cluster 3 : orange, cluster 4 : green, cluster 5 : blue, cluster 6 : cyan) for the period 2011-2018

Such patterns suggest that, during the cold months, the three compounds fluctuations are associated with the same anthropogenic processes convoluted through the atmospheric dispersion. However, during the warm months CO_2 residuals intraseasonal variations may have different drivers than CO or CH_4 residuals or scale footprints are different. For example

natural biospheric contributions from different scales (local to continental) are larger for CO_2 during the warm months. Photochemical reactions are also much more activated. This result suggests that biospheric CO_2 fluxes may be the dominant driver of CO_2 intraseasonal variations during the warm period while anthropogenic emissions lead the intraseasonal variations of the three compounds during the cold period.

5. Conclusion

The OPE station is a new atmospheric station that was set up in 2011 as part of the ICOS Demo Experiment. It is a continental station sampling air-masses influenced within regional footprints. In addition to greenhouse gases and meteorological parameters mandatory for ICOS, the station measures aerosol properties, radioactivity and is part of the regional air quality network. The greenhouse gases measurements are performed in compliance with the ICOS atmospheric station specifications, and the station was labelled by ICOS-ERIC in 2017. We presented the GHG measurement system as well as the quality control performed. Then analysis of the diurnal cycles, seasonal cycles and trends were shown for the GHG data over the 2011-2018 period. Lastly we analysed the compounds residuals with regard to the air masses history.

The monthly mean field CMR were estimated between 0.01 and 0.04 ppm for CO_2, 0.14 and 0. 5 ppb for CH_4 and 0.1 and 5.4 ppb for CO. The monthly mean field LTR were estimated between 0.003 and 0.013 ppm for CO_2, between 0.03 and 0.23 ppb for CH_4, and between 0.14 and 2.17ppb for CO. Biases estimated from the station working standards or by the cucumbers intercomparison are between ±0.1 ppm for CO_2, ±0.75 ppb for CH_4 and ±5 ppb for CO since 2016.

The station was audited twice, once just after its start in 2011 and then in 2014. In 2011, the field audit revealed a median difference of 0.13 ppm for CO_2 and of 0.4 ppb for CH_4. During the 2014 audit, the mean biases were between 0.03 and 0.05 ppm for CO_2 and between 0.7 and 1.8 ppb for CH_4. The audits results as well as the routine quality control metrics such as CMR, LTR and biases, and the cucumbers intercomparisons showed that the OPE station reached the compatibility goals defined by the WMO for CO_2, CH_4, and CO for most of the time between 2011 and 2018 (WMO, 2011). The station set-up and its standard operating procedures are also fully compliant with the ICOS specifications (Laurent et al.,. 2017).

The diurnal cycles of the three compounds show the amplification of the vertical gradient at night mainly caused by the night-time boundary layer stratification associated with ground cooling and radiative loss. Minimum values are reached during the afternoon when vertical mixing is more efficient. In addition to this main atmospheric dynamics influence, diurnal cycles of the surface emissions and of the chemical processes also play some roles in the diurnal profiles of the three compounds. We focused on the afternoon data as we are interested in larger scale processes. We computed the mean seasonal cycles of CO_2, CH_4 and CO. In addition relatively strong positive trends were observed for CO_2 and CH_4 with a mean annual growth rate of 2.4 ppm/year and 8.8 ppb/year respectively for the period 2011-2018. No significant trend was observed for CO.

The residuals from the trends and seasonal cycles identified by the time series decompositions are much stronger during the cold period (October to March) than during the warm period (April to September.) Our analysis of the residuals highlights the major influence of air masses on the atmospheric compositions residuals. Air masses originating from the western quadrant

with an Atlantic Ocean signature are associated with the lowest residual variability. Eastern continental air masses or stagnant situations are associated with larger residuals and high variability. The correlations between the compounds residuals are also stronger during the cold period. Furthermore, there are no significant correlation between CO_2 and CO or CH_4 during the warm period. This shows that summer CO_2 residuals have important natural sources while anthropogenic drivers dominate CO and CH_4 variations.

Acknowledgements

The authors gratefully acknowledge the NOAA Air Resources Laboratory (ARL) for the provision of the HYSPLIT transport and dispersion model and/or READY website (http://www.ready.noaa.gov) used in this publication. S. Hammer from Heidelberg University and H. Aaltonen from FMI are thanked for their efforts during the OPE station audits. Staff from IRFU-CEA are acknowledged for their contribution to the station's initial design and installation. We also thank staff from SNO-ICOS-France and from the ICOS Atmospheric Thematic Center for their technical support.

Competing interests: The authors declare that they have no conflict of interest.

References

Bergamaschi, P., Karstens, U., Manning, A. J., Saunois, M., Tsuruta, A., Berchet, A., Vermeulen, A. T., Arnold, T., Janssens-Maenhout, G., Hammer, S., Levin, I., Schmidt, M., Ramonet, M., Lopez, M., Lavric, J., Aalto, T., Chen, H., Feist, D. G., Gerbig, C., Haszpra, L., Hermansen, O., Manca, G., Moncrieff, J., Meinhardt, F., Necki, J., Galkowski, M., O'Doherty, S., Paramonova, N., Scheeren, H. A., Steinbacher, M., and Dlugokencky, E.: Inverse modelling of European CH4 emissions during 2006–2012 using different inverse models and reassessed atmospheric observations, Atmos. Chem. Phys., 18, 901-920, https://doi.org/10.5194/acp-18-901-2018, 2018

Berhanu, T. A., Satar, E., Schanda, R., Nyfeler, P., Moret, H., Brunner, D., Oney, B., and Leuenberger, M.: Measurements of greenhouse gases at Beromünster tall-tower station in Switzerland, Atmos. Meas. Tech., 9, 2603-2614, https://doi.org/10.5194/amt-9-2603-2016, 2016

Broquet, G., Chevallier, F., Bréon, F.-M., Kadygrov, N., Alemanno, M., Apadula, F., Hammer, S., Haszpra, L., Meinhardt, F., Morguí, J. A., Necki, J., Piacentino, S., Ramonet, M., Schmidt, M., Thompson, R. L., Vermeulen, A. T., Yver, C., and Ciais, P.: Regional inversion of CO2 ecosystem fluxes from atmospheric measurements: reliability of the uncertainty estimates, Atmos. Chem. Phys., 13, 9039-9056, https://doi.org/10.5194/acp-13-9039-2013, 2013.

Carslaw DC, Ropkins K : openair — An R package for air quality data analysis. Environmental Modelling & Software, 27–28(0), 52–61, 2012

El Yazidi, A., Ramonet, M., Ciais, P., Broquet, G., Pison, I., Abbaris, A., Brunner, D., Conil, S., Delmotte, M., Gheusi, F., Guerin, F., Hazan, L., Kachroudi, N., Kouvarakis, G., Mihalopoulos, N., Rivier, L., and Serça, D.: Identification of spikes associated with local sources in continuous time series of atmospheric CO, CO_2 and CH_4, Atmos. Meas. Tech., 11, 1599-1614, https://doi.org/10.5194/amt-11-1599-2018, 2018.

Hammer, S., Konrad, G., Vermeulen, A. T., Laurent, O., Delmotte, M., Jordan, A., Hazan, L., Conil, S., and Levin, I.: Feasibility study of using a "travelling" CO_2 and CH_4 instrument to validate continuous in situ measurement stations, Atmos. Meas. Tech., 6, 1201-1216, https://doi.org/10.5194/amt-6-1201-2013, 2013

Hazan, L., Tarniewicz, J., Ramonet, M., Laurent, O., and Abbaris, A.: Automatic processing of atmospheric CO_2 and CH_4 mole fractions at the ICOS Atmosphere Thematic Centre, Atmos. Meas. Tech., 9, 4719-4736, https://doi.org/10.5194/amt-9-4719-2016, 2016

Heid, L., Calvaruso, C., Andrianantenaina, A. Granier A., Conil S., Rathberger C., Turopault M.P., Longdoz B. : Seasonal time-course of the above ground biomass production efficiency in beech trees (Fagus sylvatica L.). Annals of Forest Science 75: 31. https://doi.org/10.1007/s13595-018-0707-9, 2018

Kadygrov, N., Broquet, G., Chevallier, F., Rivier, L., Gerbig, C., and Ciais, P.: On the potential of the ICOS atmospheric CO_2 measurement network for estimating the biogenic CO_2 budget of Europe, Atmos. Chem. Phys., 15, 12765-12787, https://doi.org/10.5194/acp-15-12765-2015,

Kountouris, P., Gerbig, C., Rödenbeck, C., Karstens, U., Koch, T. F., and Heimann, M.: Atmospheric CO2 inversions on the mesoscale using data-driven prior uncertainties: quantification of the European terrestrial CO2 fluxes, Atmos. Chem. Phys., 18, 3047-3064, https://doi.org/10.5194/acp-18-3047-2018, 2018

Kromer B., Münnich K.O.: Co2 Gas Proportional Counting in Radiocarbon Dating — Review and Perspective. In: Taylor R.E., Long A., Kra R.S. (eds) Radiocarbon After Four Decades. Springer, New York, NY,1992

Laurent, O.: ICOS Atmospheric Station Specifications, ICOS technical report (publicly available on https://icos-atc.lsce.ipsl.fr/doc_public), 2017

Le Quéré, C. and coauthors: Global Carbon Budget 2018, Earth System Science Data, 10, 1-54, 2018, DOI: 10.5194/essd-10-2141-2018

Lebegue, B., Schmidt, M., Ramonet, M., Wastine, B., Yver Kwok, C., Laurent, O., Belviso, S., Guemri, A., Philippon, C., Smith, J., and Conil, S.: Comparison of nitrous oxide (N_2O) analyzers for high-precision measurements of atmospheric mole fractions, Atmos. Meas. Tech., 9, 1221-1238, https://doi.org/10.5194/amt-9-1221-2016, 2016

Leip A, Skiba U, Vermeulen A, Thompson RL.:. A complete rethink is needed on how greenhouse gas emissions are quantified for national reporting. Atmospheric Environment. 174:237-240. https://doi.org/10.1016/j.atmosenv.2017.12.006; 2018

Levin, I., Münnich, K., Weiss, W.: The Effect of Anthropogenic CO_2 and 14C Sources on the Distribution of 14C in the Atmosphere. Radiocarbon, 22(2), 379-391. doi:10.1017/S003382220000967X,1980

Lopez, M., Schmidt, M., Ramonet, M., Bonne, J.-L., Colomb, A., Kazan, V., Laj, P., and Pichon, J.-M.: Three years of semicontinuous greenhouse gas measurements at the Puy de Dôme station (central France), Atmos. Meas. Tech., 8, 3941-3958, https://doi.org/10.5194/amt-8-3941-2015, 2015

Lowry D., Lanoisellé M.E., Fisher R. E., Martin M., Fowler C. M. R., France J. L., Hernández-Paniagua1 I. Y., Novelli P.C., Sriskantharajah S., O'Brien P., Rata N.D., Holmes C.W., Fleming Z. L., Clemitshaw K. C., Zazzeri G., Pommier M., McLinden C. A. and Nisbet E.G.: Marked long-term decline in ambient CO mixing ratio in SE England, 1997–2014: evidence of policy success in improving air quality. Sci. Rep. 6, 25661; doi: 10.1038/srep25661, 2016

Nisbet, E. G., Manning, M. R., Dlugokencky, E. J., Fisher, R. E., Lowry, D., Michel, S. E., et al: Very strong atmospheric methane growth in the 4 years 2014–2017: Implications for the Paris Agreement. Global Biogeochemical Cycles, 33. https://doi.org/10.1029/2018GB006009, 2019

Peters, G. P., Le Quéré, C., Andrew, R. M., Canadell, J. G., Friedlingstein, P., Ilyina, T., Jackson, R. B., Joos, F., Korsbakken, J. I., McKinley, G. A., Sitch, S., and Tans, P.: Towards real-time verification of CO2 emissions, Nat. Clim. Change, 7, 848–850, https://doi.org/10.1038/s41558-017-0013-9, 2017

Pison, I., Berchet, A., Saunois, M., Bousquet, P., Broquet, G., Conil, S., Delmotte, M., Ganesan, A., Laurent, O., Martin, D., O'Doherty, S., Ramonet, M., Spain, T. G., Vermeulen, A., and Yver Kwok, C.: How a European network may help with

estimating methane emissions on the French national scale, Atmos. Chem. Phys., 18, 3779-3798, https://doi.org/10.5194/acp-18-3779-2018, 2018

Rella, C. W., Chen, H., Andrews, A. E., Filges, A., Gerbig, C., Hatakka, J., Karion, A., Miles, N. L., Richardson, S. J., Steinbacher, M., Sweeney, C., Wastine, B., and Zellweger, C.: High accuracy measurements of dry mole fractions of carbon dioxide and methane in humid air, Atmos. Meas. Tech., 6, 837-860, https://doi.org/10.5194/amt-6-837-2013, 2013

Satar, E., Berhanu, T. A., Brunner, D., Henne, S., and Leuenberger, M.: Continuous CO_2/CH_4/CO measurements (2012–2014) at Beromünster tall tower station in Switzerland, Biogeosciences, 13, 2623-2635, https://doi.org/10.5194/bg-13-2623-2016, 2016

Schibig, M. F., Steinbacher, M., Buchmann, B., van der Laan-Luijkx, I. T., van der Laan, S., Ranjan, S., and Leuenberger, M. C.: Comparison of continuous in situ CO_2 observations at Jungfraujoch using two different measurement techniques, Atmos. Meas. Tech., 8, 57-68, https://doi.org/10.5194/amt-8-57-2015, 2015

Schmidt, M., Lopez, M., Yver Kwok, C., Messager, C., Ramonet, M., Wastine, B., Vuillemin, C., Truong, F., Gal, B., Parmentier, E., Cloué, O., and Ciais, P.: High-precision quasi-continuous atmospheric greenhouse gas measurements at Trainou tower (Orléans forest, France), Atmos. Meas. Tech., 7, 2283-2296, https://doi.org/10.5194/amt-7-2283-2014, 2014

Sen, P.K.: Estimates of the regression coefficient based on Kendall's tau, Journal of the American Statistical Association, 63 (324): 1379–1389, doi:10.2307/2285891, 1968.

Thoning, K.W., P.P. Tans, and W.D. Komhyr, Atmospheric carbon dioxide at Mauna Loa Observatory, 2. Analysis of the NOAA/GMCC data, 1974 1985., J. Geophys. Res. ,94, 8549 8565,1989

Vardag, S. N., Hammer, S., O'Doherty, S., Spain, T. G., Wastine, B., Jordan, A., and Levin, I.: Comparisons of continuous atmospheric CH_4, CO_2 and N_2O measurements – results from a travelling instrument campaign at Mace Head, Atmos. Chem. Phys., 14, 8403-8418, https://doi.org/10.5194/acp-14-8403-2014, 2014

Turner, A.J., Frankenberg, C., Kort, E.A.: Interpreting contemporary trends in atmospheric methane, Proc. Natl. Acad. Sci., 116 (8) 2805-2813; DOI: 10.1073/pnas.1814297116, 2019

Vermeulen, A. T., Hensen, A., Popa, M. E., van den Bulk, W. C. M., and Jongejan, P. A. C.: Greenhouse gas observations from Cabauw Tall Tower (1992–2010), Atmos. Meas. Tech., 4, 617-644, https://doi.org/10.5194/amt-4-617-2011, 2011

WMO: Report of the 15th WMO/IAEA Meeting of Experts on Carbon Dioxide, other Greenhouse Gases and Related Tracers Measurement Techniques, 7–10 September 2009, GAW Report No. 194, WMO TD No. 1553, 2011

Yuan, Y., Ries, L., Petermeier, H., Trickl, T., Leuchner, M., Couret, C., Sohmer, R., Meinhardt, F., and Menzel, A.: On the diurnal, weekly, and seasonal cycles and annual trends in atmospheric CO2 at Mount Zugspitze, Germany, during 1981–2016, Atmos. Chem. Phys., 19, 999-1012, https://doi.org/10.5194/acp-19-999-2019, 2019

Yver Kwok, C., Laurent, O., Guemri, A., Philippon, C., Wastine, B., Rella, C. W., Vuillemin, C., Truong, F., Delmotte, M., Kazan, V., Darding, M., Lebègue, B., Kaiser, C., Xueref-Rémy, I., and Ramonet, M.: Comprehensive laboratory and field testing of cavity ring-down spectroscopy analyzers measuring H_2O, CO_2, CH_4 and CO, Atmos. Meas. Tech., 8, 3867-3892, https://doi.org/10.5194/amt-8-3867-2015, 2015.

Zellweger, C., Emmenegger, L., Firdaus, M., Hatakka, J., Heimann, M., Kozlova, E., Spain, T. G., Steinbacher, M., van der Schoot, M. V., and Buchmann, B.: Assessment of recent advances in measurement techniques for atmospheric carbon dioxide and methane observations, Atmos. Meas. Tech., 9, 4737-4757, https://doi.org/10.5194/amt-9-4737-2016, 2016